

Optical symmetries and anisotropic transport in high- T_c superconductors

T.P. Devereaux

Department of Physics, University of Waterloo, Waterloo, ON, N2L 3G1, Canada

(Dated: November 8, 2018)

A simple symmetry analysis of in-plane and out-of-plane transport in a family of high temperature superconductors is presented. It is shown that generalized scaling relations exist between the low frequency electronic Raman response and the low frequency in-plane and out-of-plane conductivities in both the normal and superconducting states of the cuprates. Specifically, for both the normal and superconducting state, the temperature dependence of the low frequency B_{1g} Raman slope scales with the c -axis conductivity, while the B_{2g} Raman slope scales with the in-plane conductivity. Comparison with experiments in the normal state of Bi-2212 and Y-123 imply that the nodal transport is largely doping independent and metallic, while transport near the BZ axes is governed by a quantum critical point near doping $p \sim 0.22$ holes per CuO_2 plaquette. Important differences for La-214 are discussed. It is also shown that the c -axis conductivity rise for $T \ll T_c$ is a consequence of partial conservation of in-plane momentum for out-of-plane transport.

PACS numbers: 74.25.Jb, 71.27.+a, 78.30-j

I. INTRODUCTION

The strong anisotropy of in-plane (ab) and out-of-plane (c) transport in the cuprate systems revealed by angle-resolved photoemission spectroscopy (ARPES), NMR, resistivity, Hall, Raman, and optical conductivity measurements is as unresolved and longstanding a problem as superconductivity itself^{1,2,3,4,5,6,7,8}. As a function of hole doping per CuO_2 plaquette p the ab -plane resistivity $\rho_{ab}(T)$ (Fig. 1A) shows a metallic temperature dependence ($d\rho/dT > 0$) for a wide range of doping while the c -axis resistivity $\rho_c(T)$ (Fig. 1B) varies as T^r with an exponent r that changes from 2 to -2 as p decreases. The resistivity ratio $\rho_c(T)/\rho_{ab}(T)$ is large and becomes increasingly temperature dependent in all (hole-doped) cuprate systems for p below $\simeq 0.22$ at low temperatures^{2,3,4,5,6,7,8}.

It was pointed out early on that the c -axis properties provided an useful spectral tool to examine in-plane charge dynamics⁹. As a result, many approaches have been put forward to address the nature of in-plane versus out-of-plane transport in terms of anisotropy of the in-plane quasiparticle (qp) self energies $\Sigma(\mathbf{k}, T)$, c -axis hopping $t_{\perp}(\mathbf{k})$, impurity assisted hopping, interband transitions, or deconfinement of electrons^{9,10,11,12,13,14,15,16,17,18,19,20,21}. Recently the issue of spectral weight transfers in optical conductivity measurements brought about by superconductivity has attracted a great deal of attention^{7,8,9,10}. The mechanism by which 3D superconducting phase coherence sets in is of continued interest and debate which has been guided in a large part by the measurements of the c -axis transport properties.

The issue is still largely unsettled basically due to the open question of whether electron hopping in the out-of-plane direction is coherent^{6,7,8,9,10,11}. If there were an at least partial conservation of the in-plane momentum for qp tunnelling along the c -axis, LDA²² would indeed predict an interrelation between c -axis transport and the qp scattering rate close to $(\pi, 0)$ in the Brillouin zone (BZ).

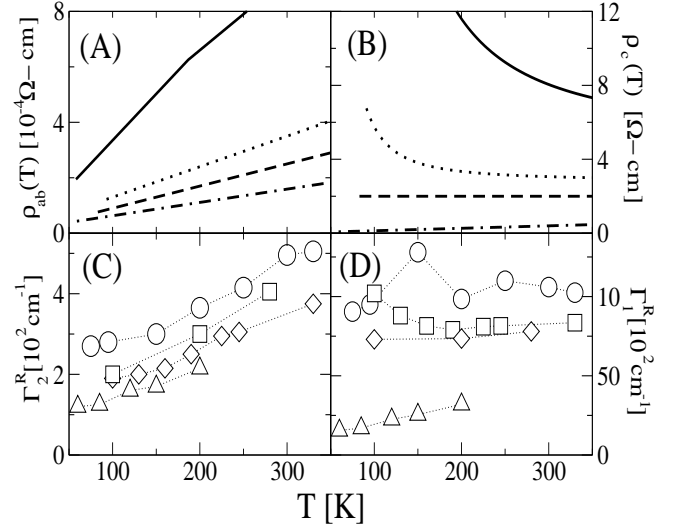


FIG. 1: Experimental results for Bi-2212 for $\rho_{ab}(T)$ (Panel A), $\rho_c(T)$ (Panel B), the Raman-derived B_{2g} , B_{1g} qp relaxation rate $\Gamma_{2,1}^R$ (Panel C, Panel D), respectively. The solid lines, circles correspond to underdoped samples ($p = 0.10$) with $T_c \sim 57\text{K}$, dotted lines, squares correspond to optimally doped samples ($p = 0.15$) with $T_c \sim 92\text{K}$, dashed lines, diamonds correspond to slightly overdoped samples ($p = 0.19$) with $T_c \sim 82\text{K}$, and the dotted-dashed lines, triangles correspond to overdoped samples ($p = 0.23$) with $T_c \sim 52\text{K}$. All resistivities were measured in Ref.⁴, except for the overdoped ($T_c = 52\text{K}$) sample which was measured in Ref.⁵. The Raman qp relaxation rates are taken from Ref.²⁵.

What would be extremely useful would be a transport measurement beside conductivity which might directly test whether transport in the plane is intimately tied to out-of-plane transport.

A behavior similar to the resistivity anisotropy is reflected in electronic Raman scattering measurements when comparing the temperature dependence of the low energy continuum measured in B_{1g} polarization orien-

tations, which project out charge fluctuations near the BZ axes, to B_{2g} configurations, which probe charge fluctuations along the BZ diagonals. Hackl *et al.*²³ and Blumberg and Klein²⁴ have pointed out the close connection between B_{2g} Raman and in the ab-plane conductivity. Further, Opel *et al.*²⁵ and Venturini *et al.*²⁶ compared the Raman relaxation rate in each channel, defined as the inverse of the slope of the low energy Raman response $\Gamma_{1,2}^R = \lim_{\Omega \rightarrow 0} [\partial \chi''_{\gamma,\gamma}(\Omega, T) / \partial \Omega]^{-1}$. For both $\text{YBa}_2\text{Cu}_3\text{O}_{7-\delta}$ (Y-123) and $\text{Bi}_2\text{Sr}_2\text{CaCu}_2\text{O}_{8+\delta}$ (Bi-2212), it was found that for B_{2g} symmetry, Γ_2^R (Fig. 1C) approximately scales with $\rho_{ab}(T)$ over a wide doping range, while for B_{1g} , Γ_1^R (Fig. 1D) was found to cross over from metallic to insulator behavior for p less than ~ 0.22 , occurring at higher dopings than that usually attributed to the formation of a pseudogap⁸. This has recently been interpreted as evidence for an underlying quantum critical point lying near $p_c \simeq 0.22$ of an unconventional metal-insulator transition (MIT)²⁶.

At low frequencies for underdoped systems, $\sigma_c(T)$ for Y-123 and $\text{YBa}_2\text{Cu}_4\text{O}_8$ (Y-124) decreases rapidly with decreasing temperature²⁷. From this a pseudogap has been inferred and well-documented. A much weaker spectral weight reduction is seen for $\text{La}_{2-x}\text{Sr}_x\text{CuO}_4$ (La-214)²⁸. Contrary to the out-of-plane conductivity, it is widely believed that there is no direct indication of a pseudogap in σ_{ab} ²⁹. The weak dependence with temperature of the *ab*-plane optical sum rule compared the rapid decrease at low temperature of the integrated *c*-axis conductivity has been interpreted in Ref.¹⁰ qps located near $(\pi, 0)$ from the anisotropy of t_{\perp} .

Raman scattering has been widely used to address the pseudogap. Recently, the presence of a pseudogap has been derived from *c*-axis A_{1g} Raman measurements in Y-124³⁰. A much weaker signature of a pseudogap is seen in the B_{2g} channel in Y-123 and Bi-2212^{25,31}. In optimal and overdoped systems, pair-breaking features appear only when superconducting coherence is established and their location at different energies for different symmetry channels has been well documented and interpreted as Cooper pairs having $d_{x^2-y^2}$ symmetry and well defined low energy qp excitations^{32,33}. While the B_{2g} pair-breaking feature appears at and scales with T_c for all dopings considered, closer to optimal doping and for underdoped systems, low frequency spectral weight is lost at low temperatures and the B_{1g} pair-breaking peak becomes difficult to distinguish from the background^{25,30,31,32,33,34,35,36,37,38}. This loss of spectral weight with temperature is very similar to the behavior seen in Raman scattering in Kondo and mixed-valent insulators and is indicative of gapped excitations³⁹.

In the superconducting state, the temperature dependence of the *ab*-plane low frequency (or regular part of the dc) conductivity^{40,41} typically shows a peak around 35K which is material dependent and has been attributed to the rapid collapse of the quasiparticle (qp) inelastic scattering rate below T_c and the rise of the qp elastic scattering rate for low T ^{42,43,44,45}. A similar peak seen in

in-plane thermal conductivity measurements was found to be sensitive to annealing conditions⁴⁶. The *c*-axis low frequency conductivity in $\text{YBa}_2\text{Cu}_3\text{O}_{6.95}$ meanwhile does not show a peak in this region but has an upturn at temperatures below 25K. The origin of the peak is currently not understood^{14,47}. The *c*-axis thermal conductivity was found to show a very weak peak also sensitive to annealing conditions⁴⁶. Much less is known about the temperature dependence of Raman scattering in the static limit in the superconducting state, although some theoretical treatments have appeared^{33,48}. One would like to test whether features shown in conductivity measurements are found in Raman scattering measurements and vice-versa.

Shastri and Shraiman have noted the close similarity between the conductivity and the Raman response and have suggested a scaling relation exists between the two which follow the same temperature and frequency dependence⁴⁹:

$$\Omega \sigma'(\Omega, T) = A \chi''(\Omega, T), \quad (1)$$

with A a constant independent of frequency and temperature. This Shastri-Shraiman (SS) relation holds if the qp self energy Σ is independent of \mathbf{k} and has been shown to be exact for both the Falicov-Kimball⁵⁰ and Hubbard⁵¹ models in the limit of large dimensions where the self energy and vertex corrections are local. Generally though any \mathbf{k} -dependence of Σ and/or the irreducible Raman or current vertices invalidates the SS scaling relation making it inappropriate for strongly anisotropic systems such as the cuprates.

However, an approximate scaling relation may hold for certain cases and one purpose of this paper is to point out some of the connections between the conductivity and Raman response for strongly anisotropic systems and derive appropriate scaling relations. In particular we will, based on symmetry arguments, determine that a variant of the SS relation can be formulated to show that a scaling relation exists separately between σ_{ab} and $1/\Gamma_2^R$ and between σ_c and $1/\Gamma_1^R$ as a consequence of the momentum dependence of $t_{\perp}(\mathbf{k})$, in-plane self energy $\Sigma(\mathbf{k})$, and a $d_{x^2-y^2}$ energy gap $\Delta(\mathbf{k})$. These scaling relations are also found to also hold in the superconducting state. Comparison with the available data on Y-123 and Bi-2212 in the normal state suggests that qps located near the BZ axes or ‘‘hot spots’’ become gapped above optimal doping²⁶ while the qps located along the BZ diagonals or ‘‘cold spots’’ are largely doping independent and remain metallic. Thus the *c*-axis transport is partially influenced by a correlation gap near $(\pi, 0)$ because of partial conservation of the in-plane momentum in *c*-axis transport and not completely by *c*-axis diffusion. There are important differences however with La-214. Various models for qp scattering as a function of doping are discussed, and it is found that generally no single model can adequately capture the complex nature of electron dynamics over a wide range of doping. Features of the theory in the superconducting state qualitatively describe the behavior

seen in the c -axis conductivity, but there are important questions left unanswered. In conclusion, experimental evidence in both the normal and superconducting states suggest that the in-plane momentum is at least partially conserved in c -axis transport over a very wide doping range.

The plan of the paper is as follows: Sections II and III present the formalism used and the results for the temperature dependence of the low frequency in-plane and out-of-plane conductivity and Raman response in the normal and superconducting states, respectively, for the common model where t_{\perp} vanishes along the BZ diagonals, summarized in the Appendix. The results are summarized and open points are discussed in Section IV.

II. NORMAL STATE

A. Formalism

The quantum chemistry of the tetragonal Cu-O system yields an out-of-plane hopping which is modulated by the in-plane momentum in such a way that it is strongly governed by qps located along the BZ axes as opposed to qps along the zone diagonal, $t_{\perp}(\mathbf{k}) = t_{\perp}^0 [\cos(k_x a) - \cos(k_y a)]^2$, as reviewed in the Appendix. This form for the hopping has been widely used to study the penetration depth¹³, c -axis conductivity^{7,14,15}, and bi-layer splitting²² in ARPES¹. However we note that inclusion of the Cu-O chains or O displacements would lower the symmetry with the consequence that the out-of-plane hopping would no longer vanish along the BZ diagonals which could only be noticeable at very low temperatures. We now explore the consequences of such a term on the regular part of the dc conductivities and the symmetry-dependent electronic Raman response for qp scattering in the $a-b$ plane and along the c -axis in the following sections.

In linear response theory, expressions for the regular part of the conductivity and Raman response in the absence of vertex corrections are given as (here and throughout we set $k_B = \hbar = 1$)

$$\begin{aligned} \begin{pmatrix} \Omega \sigma'_{\alpha,\beta}(\Omega) \\ \chi'_{\gamma,\gamma}(\Omega) \end{pmatrix} &= \int \frac{dx}{\pi} [f(x) - f(x + \Omega)] \\ &\times \sum_{\mathbf{k}} \begin{pmatrix} j_{\mathbf{k}}^{\alpha} j_{\mathbf{k}}^{\beta} \\ \gamma_{\mathbf{k}}^2 \end{pmatrix} G_{\mathbf{k}}^R(x) G_{\mathbf{k}}^A(x + \Omega). \end{aligned} \quad (2)$$

Here f is the Fermi function, $G^{R,A}$ are the retarded, advanced Green's functions, respectively, $j_{\mathbf{k}}^{\alpha} = e \frac{\partial \epsilon_{\mathbf{k}}}{\partial k_{\alpha}}$ is the current vertex for direction α given in terms of the band dispersion $\epsilon_{\mathbf{k}}$ and electron charge e , and $\gamma_{\mathbf{k}}$ is the Raman vertex set by choosing the incoming and outgoing light polarization vectors.

The inclusion of vertex corrections is crucial for satisfying Ward identities for the conductivity and particle number conservation for the charge density response.

They convert scattering lifetimes into transport lifetimes, and also add an additional source of momentum and temperature dependence to the corresponding response functions. Vertex corrections have been recently been considered in FLEX treatments of the Hubbard model⁵² and a spin-fermion model⁵³ where it was shown the B_{1g} Raman irreducible vertex is highly renormalized near the $(\pi, 0)$ regions of the BZ. In addition vertex corrections have been calculated exactly in the limit of large dimensions for the Falicov-Kimball model, where it was shown they are important in the A_{1g} channel to properly lead to gauge invariance and particle-number conservation but do not contribute to other channels⁵⁰. Generally, vertex corrections have not yet been generically or systematically investigated in 2D and we thus neglect them since we are interested in exploring simple symmetry properties of the various experimental probes.

The current vertices are simply $j_{\mathbf{k}}^x = v_x \sin(k_x a)$, and $j_{\mathbf{k}}^z = v_z [\cos(k_x a) - \cos(k_y a)]^2$, where $v_x \sim t$ and $v_z \sim t_{\perp}^0$ have only a mild momentum dependence. In the limit where the incident and scattered photon energies are small compared to the bandwidth the Raman vertex is given as the curvature of the band: $\gamma_{\alpha,\beta} = \frac{\partial^2 \epsilon(\mathbf{k})}{\partial k_{\alpha} \partial k_{\beta}}$ ⁵⁴. The vertices are thus determined from the above band structure as $\gamma_{\mathbf{k}} = b_1 [\cos(k_x a) - \cos(k_y a)]$, $b_2 \sin(k_x a) \sin(k_y a)$ for B_{1g}, B_{2g} orientations, respectively, while for c -axis A_{1g} Raman $\gamma_{\mathbf{k}} = a_{zz} \cos(k_z c) [\cos(k_x a) - \cos(k_y a)]^2$. The prefactors $b_1 \sim t$, $b_2 \sim t'$, and $a_{zz} \sim t_{\perp}^0$ can also be assumed to be only mildly frequency dependent corresponding to off-resonant scattering and therefore are only multiplicative constants. Since the energy range considered is very small in comparison to all electronic bandwidths involved the assumption $b_{1,2}$ and a_{zz} to be constant is robust under all realistic circumstances.

As can be seen by the weighting of the vertices, we may expect similar behavior for the B_{2g} Raman and in-plane conductivity, and the B_{1g} , c -axis A_{1g} Raman, and the out-of-plane conductivity as well. The former two quantities assign weight around the Fermi surface (FS) to the diagonals while the latter three assign weight along the zone axes.

In correlated electron systems the density of states (DOS) plays a strong role in determine transport properties. In Mott insulators, charge transport occurs via excitations across a Mott gap from the lower to upper Hubbard bands, while in metallic systems the DOS near the Fermi level plays the dominant role in low frequency transport. The nature of how the density states evolves across a MIT has been an issue of intense debate for a large number of years as few exact results are available. However, in the limit of large dimensions dynamical mean field theory has a great deal of insight for some model Hamiltonians⁵⁵. Away from half-filling the Hubbard model and the Falicov-Kimball both possess metallic ground states. The DOS has a typical three-peak structure: the separated upper and lower Hubbard bands and a qp DOS at the Fermi level emerging from the Abrikosov-Suhl resonance in the related impurity prob-

lem. As the system approaches half-filling and/or for larger values of U at fixed filling, the qp DOS generally diminishes and vanishes in the Mott insulating phase as spectral weight is transferred into the Hubbard bands. Capturing this transfer in models in realistic dimensions is one of the most important and difficult problem in condensed matter physics.

We thus consider charge transport in correlated systems having coherent qps as well as large energy incoherent charge excitations related to the Hubbard bands. We model coherent qps near the FS by a phenomenological momentum, frequency, and temperature dependent self energy derivable in principle from a renormalizable effective low energy theory: $G_{coh,\mathbf{k}}^{R,A}(\omega) = Z_{\mathbf{k}}(\omega, T)/(\omega - \bar{\epsilon}_{\mathbf{k}} \pm i\Gamma_{\mathbf{k}}(\omega, T))$. Here $\bar{\epsilon}$ is the renormalized band structure, $Z_{\mathbf{k}}(\omega, T) = [1 - \partial\Sigma'_{\mathbf{k}}(\omega, T)/\partial\omega]^{-1}$ is the qp residue, and $\Gamma_{\mathbf{k}}(\omega, T)$ is the momentum, frequency, and temperature dependent qp scattering rate. The full Green's function also includes an incoherent part G_{inc} accounting for larger energy excitations such as those involving the lower and upper Hubbard bands. In what follows we focus on low frequency transport in metallic phases and neglect G_{inc} and singularities of the self energy indicative of an incipient phase transition.

Converting the momentum sum to an integral over an infinite band we obtain in the limit of low frequencies

$$\left(\frac{\sigma'_{\alpha,\beta}(\Omega \rightarrow 0, T)}{\partial\chi''_{\gamma,\gamma}(\Omega \rightarrow 0, T)/\partial\Omega} \right) = -2N_F \int dx \frac{\partial f(x)}{\partial x} \times \left\langle \left(\frac{j_{\mathbf{k}}^{\alpha} j_{\mathbf{k}}^{\beta}}{\gamma_{\mathbf{k}}^2} \right) \frac{Z_{\mathbf{k}}^2(x, T) \Gamma_{\mathbf{k}}(x, T)}{\Omega^2 + [2\Gamma_{\mathbf{k}}(x, T)]^2} \right\rangle, \quad (3)$$

where N_F is the density of states per spin at the Fermi level and $\langle \dots \rangle$ denotes performing an average over the FS. It can be immediately seen that the SS relation Eq. (1) follows if Γ is independent of momentum, as it is in local theories^{50,51,55}. In what follows we neglect specific features on and off the FS (such as van Hove) and approximate the 2D FS as a circle and expand the c -axis dispersion for small t_{\perp}^0 to obtain:

$$\begin{aligned} xx \text{ Conductivity,} & \quad j^x = v_F \sin(\phi), \\ zz \text{ Conductivity,} & \quad j^z = v_z \cos^2(2\phi), \\ B_{1g} \text{ Raman,} & \quad \gamma_{B_{1g}} = b_1 \cos(2\phi), \\ B_{2g} \text{ Raman,} & \quad \gamma_{B_{2g}} = b_2 \sin(2\phi), \\ zz \text{ } A_{1g} \text{ Raman,} & \quad \gamma_{A_{1g},zz} = a_{zz} \cos^2(2\phi) \end{aligned} \quad (4)$$

We note that the c -axis conductivity and $\partial\chi''_{A_{1g},zz}/\partial\Omega$ are given by the same expressions, in accordance with the qp scattering rate not having a k_z dependence. Therefore we confirm the SS relation for the c -axis A_{1g} Raman and c -axis conductivity, respectively:

$$\lim_{\Omega \rightarrow 0} \Omega \sigma'_{zz}(T) \propto \chi''_{A_{1g},zz}(\Omega, T), \quad (5)$$

independent of the form for $\Gamma_{\mathbf{k}}$.

At low temperatures we find from Eq. (3)

$$\left(\frac{\sigma'_{\alpha,\beta}(T)}{\partial\chi''_{\gamma,\gamma}(T)/\partial\Omega} \right) = N_F \left\langle \left(\frac{j_{\mathbf{k}}^{\alpha} j_{\mathbf{k}}^{\beta}}{\gamma_{\mathbf{k}}^2} \right) \frac{Z_{\mathbf{k}}^2(T)}{2\Gamma_{\mathbf{k}}(T)} \right\rangle, \quad (6)$$

showing the interplay of anisotropies of the scattering rate and the vertices governing the response functions.

The simple expressions for σ and $\partial\chi''/\partial\Omega$ allow for a straightforward comparison of models for the qp scattering rate. We choose a generic model which describes strong scattering weighted largely along the BZ axes plus a temperature dependent scattering rate taken to be uniform around the FS:

$$\Gamma_{\mathbf{k}}(T) = \Gamma_h(T) \cos^2(2\phi) + \Gamma_c(T). \quad (7)$$

This form for the qp scattering rate has been widely employed in a number of models differing in the representations of Γ_h and Γ_c constrained only to possess the full symmetry of the lattice (A_{1g})^{16,17,18,19}. Further parameterizations of the anisotropy do not lead to appreciable differences. For the B_{2g} Raman as well as the in-plane conductivity, the vertices weight out regions of the FS where the scattering rate is small, along the FS diagonals or ‘‘cold spots’’. However, the B_{1g} and c -axis A_{1g} Raman and the out-of-plane conductivity assign no weight to the diagonals and thus will be governed by the scattering at the ‘‘hot spots’’.

Neglecting the \mathbf{k} -dependence of the qp residue $Z_{\mathbf{k}} = Z$, the resulting integrals can be easily performed to give

$$\sigma'_{xx}(T) = v_F^2 \frac{N_F Z^2}{2\Gamma_c(T)} \frac{1}{\sqrt{1 + \Gamma_h(T)/\Gamma_c(T)}}, \quad (8)$$

$$\sigma'_{zz}(T) = v_z^2 \frac{N_F Z^2}{2\Gamma_h(T)} \left\{ \frac{1}{2} - \frac{\Gamma_c(T)}{\Gamma_h(T)} \times \left(1 - \frac{1}{\sqrt{1 + \Gamma_h(T)/\Gamma_c(T)}} \right) \right\}, \quad (9)$$

$$\frac{\partial\chi''_{B_{1g}}(T)}{\partial\Omega} = b_1^2 \frac{N_F Z^2}{2\Gamma_h(T)} \times \left\{ 1 - \frac{1}{\sqrt{1 + \Gamma_h(T)/\Gamma_c(T)}} \right\}, \quad (10)$$

$$\frac{\partial\chi''_{B_{2g}}(T)}{\partial\Omega} = b_2^2 \frac{N_F Z^2}{2\Gamma_h(T)} \frac{1}{\sqrt{1 + \Gamma_h(T)/\Gamma_c(T)}} \times \left\{ 1 - \sqrt{1 + \Gamma_h(T)/\Gamma_c(T)} + \Gamma_h(T)/\Gamma_c(T) \right\}. \quad (11)$$

These results for the ab-plane and c -axis conductivity have been derived several times, most recently by Refs.^{14,15}. However here it can be seen that there is a direct connection between conductivities and Raman response functions. It is clear that the function form for the scattering rate determines the temperature dependence

of all four response functions, and that the SS relation Eq. (1) does not hold in general.

Early on, ARPES measurements yielded $\Gamma_c \ll \Gamma_h$ from smeared spectral functions seen near the BZ axes compared to the BZ diagonals¹. However, recent ARPES measurements indicated bi-layer splitting may have led to an overestimation of Γ_h ^{1,56}, but still the limit $\Gamma_c \ll \Gamma_h$ is a useful limit to explore. In this limit the response functions are

$$\sigma'_{xx}(T) = v_F^2 \frac{N_F Z^2}{2\sqrt{\Gamma_c(T)\Gamma_h(T)}}, \quad (12)$$

$$\sigma'_{zz}(T) = v_z^2 \frac{N_F Z^2}{2\Gamma_h(T)}, \quad (13)$$

$$\frac{\partial \chi''_{B_{1g}}(T)}{\partial \Omega} = b_1^2 \frac{N_F Z^2}{2\Gamma_h(T)}, \quad (14)$$

$$\frac{\partial \chi''_{B_{2g}}(T)}{\partial \Omega} = b_2^2 \frac{N_F Z^2}{2\sqrt{\Gamma_h(T)\Gamma_c(T)}}. \quad (15)$$

This directly shows the similarity between the B_{1g} Raman slope and the c -axis conductivity, and B_{2g} Raman slope and the in-plane conductivity, regardless of the functional form chosen for two contributions to the qp scattering rate. Thus in this model consistent with experiments, a variant of the SS relation for the cuprates may be expressed as

$$\begin{aligned} \lim_{\Omega \rightarrow 0} \Omega \sigma'_{xx}(T) &\propto \chi''_{B_{2g}}(\Omega, T), \\ \lim_{\Omega \rightarrow 0} \Omega \sigma'_{zz}(T) &\propto \chi''_{B_{1g}}(\Omega, T). \end{aligned} \quad (16)$$

This demonstrates how out-of-plane transport can be directly inferred from in-plane optical transport measurements. Further, this confirms the behavior shown in Fig. (1), indicating that the in-plane momentum must be at least partially conserved for transport perpendicular to the CuO_2 planes. Moreover, with Eq. (5) this indicates that the c -axis A_{1g} Raman should scale with B_{1g} Raman:

$$\lim_{\Omega \rightarrow 0} \chi''_{A_{1g,zz}}(\Omega, T) \propto \chi''_{B_{1g}}(\Omega, T). \quad (17)$$

Eqs. (16-17) are the central results of this section.

When and how might the scaling relations Eqs. (16-17) breakdown? Clearly these scaling relations result from the momentum dependence of the respective response vertices, and since they are dictated solely on symmetry grounds, changes in how one represents the momentum dependence of the vertices can only lead to qualitative effects. However, there are a number of important factors to consider. First, the inclusion of G_{inc} will change the scaling relations if there is appreciable spectral weight near the FS, but if we restrict ourselves to metallic systems and low frequencies, then these changes are expected to be small. They might however be large for a system lying near a quantum critical point and the scaling relations may be violated. Next, relating the c -axis conductivity to the A_{1g} c -axis and B_{1g} Raman requires

that the c -axis coherent hopping vanishes along the BZ diagonals. Deviations would come from incoherent diffusive hopping, or more complex coherent hopping paths such as via the Cu-O chains in Y-123, and would result in a mixing in the scaling properties for in-plane conductivity and B_{2g} Raman transport. Lastly, vertex corrections can appreciably alter the scaling relations. Vertex corrections yield transport scattering rates in place of $2\Sigma''$ as required by Ward identities, and yield a f -sum rule for the integrated conductivity proportional to minus the kinetic energy. Ward identities can be useful for the conductivity to show that vertex corrections vanish for a momentum-dependent self energy, but no Ward identities exist for Raman with crossed polarization vectors. For example, vertex corrections may renormalize even-parity momentum charge vertices (Raman) but not odd-parity current vertices (conductivity). If these scaling relations are found to hold, they would imply that vertex corrections at low frequencies and c -axis hopping along the BZ diagonals would play only a very minor role in determining low frequency transport.

B. Transport models

The scaling relations of Eq.(16) can be seen from Fig. 1 to be qualitatively obeyed. We now consider several models for $\Gamma_h(T)$ and $\Gamma_c(T)$ to explore the scaling relations Eqs.(12-15) to address the role of anisotropic qp scattering. In all models, $\Gamma_h(T)$ and $\Gamma_c(T)$ are generally constrained by the estimated width of the spectral function measured in ARPES experiments¹. In both a ‘‘cold spot’’¹⁶ and ‘‘hot spot’’ model¹⁷, $\Gamma_c(T)$ describes weakly renormalized qp scattering primarily along the FS diagonals generally of the form

$$\Gamma_c(T) = \Gamma_{imp} + T^2/T_0, \quad (18)$$

where Γ_{imp} represents elastic impurity scattering and T_0 is the energy scale of a renormalized Fermi liquid. The impurity scattering may be chosen to reproduce the extrapolated $T = 0$ resistivity and T_0 is a parameter to be chosen to fit a cross-over from T^2 to T in the resistivity. In the ‘‘hot spot’’ model^{17,57}, $\Gamma_h(T) = \sqrt{\Gamma_{hs}T}$ represents scattering with exchange of antiferromagnetic reciprocal lattice momentum \mathbf{Q} which has been widely employed to determine the optical conductivity, in-plane and Hall resistivity in relation to ARPES. However similar behavior is also obtained for scattering in systems lying near a charge ordering instability⁵⁸ or near a FS Pomeranchuk instability⁵⁹. In the ‘‘cold spot’’ model¹⁶, $\Gamma_h(T)$ is taken to be a constant Γ_{hs} presumed to arise from strong $d_{x^2-y^2}$ pairing fluctuations, and has been employed in several works to describe in-plane and out-of-plane optical conductivity and magneto-transport^{10,15,16,18}. However the microscopic origin of Γ_{hs} is unclear in this model. In the marginal Fermi liquid (MFL) model most recently described in Ref.¹⁹, $\Gamma_c(T) \sim T$ and $\Gamma_h(T) \sim \text{constant}$ due to impurity scattering in correlated systems whereby

TABLE I: Summary of the low temperature dependence of the inverse conductivities, the Raman relaxation rates Γ_μ^R and the scattering ratio defined in the text.

Response	MFL	“Hot spot”	“Cold spot”
$\Gamma_2^R(T), \sigma_{xx}^{-1}(T)$	$T^{1/2}$	$T^{5/4}$	T
$\Gamma_1^R(T), \sigma_{zz}^{-1}(T)$	constant	$T^{1/2}$	constant
$\Gamma_1^R/\Gamma_2^R, \sigma_{xx}/\sigma_{zz}$	$T^{-1/2}$	$T^{-3/4}$	T^{-1}

strong correlation nearby a point-like scatterer induce real-space extensions of the impurity potential⁶⁰.

Following Ref.²⁵, the “Raman scattering rate” $\Gamma_\mu^R(T)$ for each channel is defined as the inverse of the Raman slope $\Gamma_\mu^R(T) = \left[\frac{\partial \chi_\mu''(\Omega \rightarrow 0, T)}{\partial \Omega} \right]^{-1}$ in order to obtain information on the single particle scattering rate on regions of the FS selected by polarization orientations $\mu = 1, 2$ for B_{1g}, B_{2g} , respectively. In the “hot spot model” we obtain $\Gamma_1^R \sim T^{1/2}$ and $\Gamma_2^R \sim T^{5/4}$, respectively, while in the “cold spot” model we obtain $\Gamma_1^R \sim \text{constant}$ and $\Gamma_2^R \sim T$, respectively. The MFL model yields $\Gamma_1^R \sim \text{constant}$ and $\Gamma_2^R \sim \sqrt{T}$, respectively. None of the models considered have presented analytic forms for the scattering rate as a function of doping, and presumably in all models Γ_h would be expected to be small in overdoped systems.

It is often useful to look at the “scattering ratio” $\Gamma_1^R(T)/\Gamma_2^R(T) \sim \rho_c(T)/\rho_{ab}(T) \sim T^{-m}$. The models discussed give $m = 1/2, 3/4$, and 1 for MFL, “hot”, and “cold” spot models, respectively. These preceding exponents are summarized in Table I. As can be seen from Fig. (1), all of these models can *qualitatively* describe the experimental results for overdoped systems, but important deviations occur for optimal and underdoped systems. The “hot spot” model yields a stronger temperature dependence however than that seen for the B_{1g} Raman and c -axis conductivity.

C. Pseudogap

The upturn of both $\Gamma_1(T)$ and $\rho_c(T)$ at low temperatures for optimal and underdoped systems is indicative of gapped qps and connected to an anisotropic pseudogap largest near the BZ axis⁸. A major issue⁶¹ is whether the pseudogap is caused by pairing without long-range phase coherence or due to loss of well defined qps at the FS related to the formation of a precursor Mott gap, or spin-density and/or charge-density wave states, for example.

In the former case, the superconducting gap amplitude closes at T^* while strong phase fluctuations force the superfluid density to appear at T_c ⁶². In more exotic phases emerging from Z_2 gauge theories, electrons fractionalize away from the BZ diagonals, spinons become deconfined and holons condense and become gapped⁶³. In these scenarios one might expect a feature in the spectra

appearing at a high energies which merges into the superconducting feature at T_c . It is not immediately clear whether this occurs in Raman data due to the nature of the 600 cm^{-1} peak³⁸.

In the spin and/or charge precursor scenario, anisotropic SDW and/or CDW fluctuations strongly affect the integrity of qp excitations near the BZ axes^{57,58}. Relatedly strong electron and Umklapp scattering in particular due to the nearness of a nesting condition can drive FS topological changes near the BZ axes or “hot spots” which preserve⁶⁴ or lower⁶⁵ the symmetry of the FS.

It is clear that the pseudogap is a manifestation of strong correlations regardless of which scenario is considered. Thus we take a simple approach and relate the pseudogap to a correlation gap as a precursor to the Mott insulating phase regardless of any underlying order, characterized by the development of G_{inc} involving large energy transfers across a precursor Mott gap. The gapping can thus be crudely understood as the loss of well defined qps located near the $(\pi, 0)$ regions of the FS, implying that the coherent part of the Green’s function diminishes away from the BZ diagonal.

Therefore in what follows the role of anisotropy in the qp residue Z is explored in a simple effort to model the effect of a loss of qp transport for the “hot” qps with decreasing p . Taking $Z_{\mathbf{k}}(T) = Z_h e^{-(E_g/T) \cos^2(2\Phi)}$ as a phenomenological model of angular dependent gapping of qps with an energy scale E_g , the integrals are straightforward and the result can be expressed analytically in terms of a degenerate hypergeometric function of two variables:

$$\begin{aligned} \sigma'_{xx}(T), \partial \chi''_{B_{2g}}(T)/\partial \Omega &\sim \\ \sigma'_{zz}(T), \partial \chi''_{B_{1g}}(T)/\partial \Omega &\sim \end{aligned} \quad (19)$$

$$\frac{N_F}{2\Gamma_c(T)} \left\{ \begin{array}{l} \Phi_1 \left(\frac{1}{2}, 1, 2, -\frac{\Gamma_h}{\Gamma_c(T)}, -\frac{E_g}{T} \right), \\ \Phi_1 \left(\frac{3}{2}, 1, 2, -\frac{\Gamma_h}{\Gamma_c(T)}, -\frac{E_g}{T} \right). \end{array} \right.$$

For almost all temperatures, the function can be accurately described as the previous results Eqs. (12-15) with the sole exception that $\sigma'_{zz}(T)$ Eq. (13) and $\partial \chi''_{B_{1g}}(T)/\partial \Omega$ Eq. (15) are multiplied by $e^{-2E_g/T}$. Thus we note that if qps located near the BZ axis become gapped or lose their spectral weight at the Fermi level, the B_{1g} Raman slope and c -axis conductivity will show activated behavior while the B_{2g} Raman slope and the in-plane conductivity would continue to show metallic behavior. This is qualitatively the situation found for doping levels below $p_c \sim 0.22$ in all the cuprates.

D. Comparison with experiments

The data for the Raman derived scattering ratio for Bi-2212 is shown in Fig. 2. The data are derived from the measurements shown in Fig. 1. The ratio derived

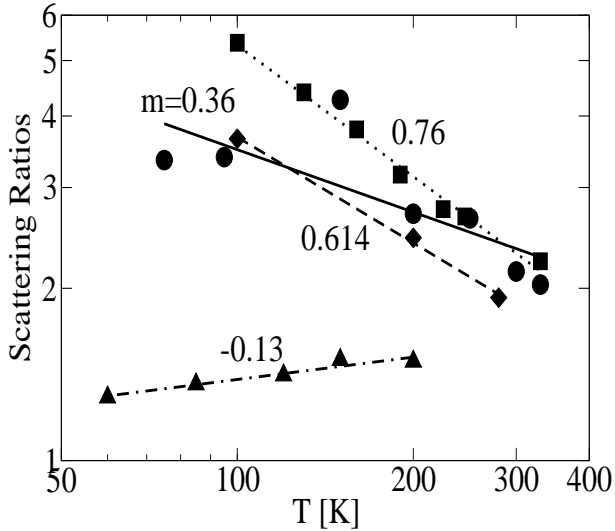


FIG. 2: A log-log plot of the Raman derived “scattering ratios” Γ_1^R/Γ_2^R (defined in the text) for Bi-2212 in Ref.²⁵ for underdoped (circles, $m = 0.36$), optimally doped (squares, $m = 0.76$), slightly overdoped (diamonds, $m = 0.614$) and appreciably overdoped (triangles, $m = -0.13$) samples shown in Fig. 1, respectively. The exponent m is determined from a least-squares fit to T^{-m} .

from the measurements on three differently doped samples of Y-123 are shown in Fig. 3. For Bi-2212 the ratio slightly increases ($m < 0$) with temperature for appreciably overdoped systems, in agreement with the results obtained for La-214⁶⁸. For decreasing doping p in both Bi-2212 and Y-123, the exponent m is positive and increases as the “hot” qps become gapped and the “cold” qps do not appreciably change. The large variation of the data from the underdoped Bi-2212 sample is due to the small intensity at low frequencies from which the slope is derived. Apart from this sample however a power-law fit adequately describes the data for both compounds. Near optimum doping both the MFL and “cold spot” model give reasonable agreement for the “scattering ratio” while on the underdoped side the “cold spot” model gives an exponent of 1 in agreement with the data on Y-123 and in rough agreement with the data on Bi-2212. An exponential dependence on temperature has been used in Refs.⁴ for the resistivity ratio to determine the magnitude of a pseudogap, for example. We note that the Raman measurements are not yet of sufficient precision to determine E_g from a fit since a straight line fit works well as shown in Fig. 2. The curvature may be obscured by the small signals measured at low frequencies however. More accurate data would be very useful.

Recent ARPES measurements have revealed that the qp self energy may not be as anisotropic as determined earlier due to the more accurate detection of bilayer splitting near the BZ axes⁵⁶. In addition, a more quantitative investigation of the qp self energy derived from recent ARPES measurements on overdoped and optimally

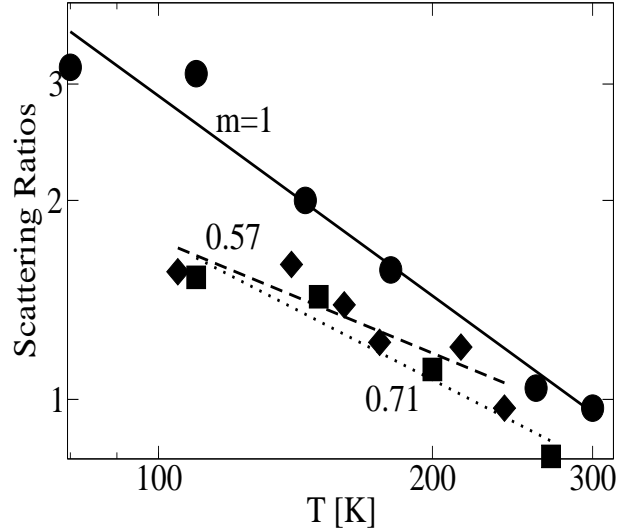


FIG. 3: A log-log plot of the data obtained in Ref.²⁵ for the Raman derived “scattering ratios” Γ_1^R/Γ_2^R (defined in the text) for YBa₂Cu₃O_{6.5} (circles, $m = 1$), YBa₂Cu₃O_{6.93} (squares, $m = 0.71$), and YBa₂Cu₃O_{6.98} (diamonds, $m = 0.57$), respectively.

doped Bi-2212⁶⁶ has been used to argue that agreement with the magnitude and temperature dependence of in-plane resistivity measurements on similar compounds can only be obtained if the transport scattering rate has no contributions from Γ_{hs} and is given solely by an MFT dependence¹⁹ on all regions of the BZ. A similar conclusion has been reached regarding the self energy and optical conductivity⁶⁷. It is however important to note that the magnitude of the derived resistivity agrees with experiment to within a factor less than two for temperatures between 100-300K. A more or less isotropic qp self energy cannot be reconciled with the Raman data unless vertex corrections are brought into play. If the experiments are taken at face value, this would imply that vertex corrections affect the Raman response and the conductivity in opposite ways: Raman vertex corrections would act to *enhance* qp scattering near the BZ axes while conductivity corrections would *decrease* it. This has the important consequence from the symmetry arguments presented above that the c -axis conductivity should then be more coherent in contrast to experiments. This lack of consistency between ARPES, ab - and c - axes conductivity, and $B_{1g,2g}$ Raman must then be traced to the detailed role of vertex corrections for each response. This work is currently in progress.

It is important to point out that the results obtained on La-214 are qualitatively different from Y-123 and Bi-2212 in underdoped systems⁶⁸. For La_{1.9}Sr_{0.1}CuO₄, a clear Fermi liquid like peak develops at low frequencies in the B_{1g} channel which sharpens as temperature is lowered so that $\partial\chi''(T)/d\Omega$ falls with decreasing temperature, similar to the behavior of the B_{2g} channel in Y-123 and Bi-2212. These features appear more or less con-

tinuously with doping. However, the peak in the B_{2g} channel seems to mimic the B_{2g} response in Y-123 and Bi-2212. We note that this is consistent with ARPES in which a more smeared spectral function is seen for $(\pi/2, \pi/2)$ rather than $(\pi, 0)$ crossings⁶⁹. Recently strong far infrared peaks have been observed in ab-plane optical response⁷⁰ in $\text{La}_{2-x}\text{Sr}_x\text{CuO}_4$ for $x = 0.05 - 0.19$ which follow a dependence on x consistent with a coexistence of charge stripes and antiferromagnetic domains⁶². Similar strong far infrared peaks have also been observed in $\text{Bi}_2\text{Sr}_2\text{CuO}_6$ (Bi-2201)⁷¹ and interpreted⁵⁸ in terms of instabilities of a Fermi liquid to charge ordering. While this interpretation is still open to questions, both of these observations can be reconciled with Raman scattering measurements if the stripes were aligned solely along the Cu-O bond directions. Whether the stripes are conducting or insulating, and whether they are static or dynamically fluctuating, the B_{2g} Raman response would have a polarization component perpendicular to the stripes and thus would project onto incoherent qp transport channels while the B_{1g} would have a finite project of both the incident and scattering polarization light vectors along a sector of coherent, conducting excitations consistent with observations. These simple symmetry considerations would change if the stripes were thought to be fluctuating in various different orientations or rotated by 45 degrees, as evidence suggest they might for more underdoped samples. More data and further calculations are essentially needed to clarify this point. It is an important and open issue to understand why this occurs for a wide range of doping in La-214 and not Y-123 and Bi-2212.

We note that only limited experimental information exists concerning c-axis Raman measurements due to the surface problems, but recently Quilty *et al.* have shown that the low frequency c-axis Raman spectral weight in $\text{YBa}_2\text{Cu}_4\text{O}_8$ depletes as temperatures are lowered³⁰. In conjunction with the spectral weight depletion at low temperatures seen in B_{1g} measurements on the same compound³⁵, the admittedly limited experimental evidence is also consistent with $A_{1g,zz}$ and B_{1g} scaling. More data would of course be useful to check this further. In this regard it should be mentioned that there is recent evidence that the c-axis Raman may shed light on a Raman active c-axis plasmon⁷². It would be extremely useful to examine whether the plasmon would violate the scaling relation or could possibly lead to a mode-coupling which pushes the plasmon into the B_{1g} channel.

III. SUPERCONDUCTING STATE

A. Formalism

We now consider how anisotropic transport in the normal state may be reflected in the superconducting state. In particular we would like to address whether the variational of the SS relation presented in Eq. (16) holds in the superconducting state.

In the absence of vertex corrections, the expressions for the Raman response and the optical conductivity in the static limit are given in terms of the Nambu Green's functions as:

$$\left(\begin{array}{c} \sigma'_{\alpha,\beta}(T) \\ \partial\chi''_{\gamma,\gamma}(T)/\partial\Omega \end{array} \right) = 2 \sum_{\mathbf{k}} \left(\begin{array}{c} j_{\mathbf{k}}^{\alpha} j_{\mathbf{k}}^{\beta} \\ \gamma_{\mathbf{k}}^2 \end{array} \right) \quad (20)$$

$$\times \int \frac{dx}{\pi} \frac{\partial f(x)}{\partial x} \{ G_0''(\mathbf{k}, x)^2 + G_3''(\mathbf{k}, x)^2 \pm G_1''(\mathbf{k}, x)^2 \}.$$

Here $\hat{G}(\mathbf{k}, \omega) = \frac{1}{\tilde{\omega}\hat{\tau}_0 - \tilde{\epsilon}(\mathbf{k})\hat{\tau}_3 - \tilde{\Delta}(\mathbf{k})\hat{\tau}_1} = G_0(\mathbf{k}, \omega)\hat{\tau}_0 + G_1(\mathbf{k}, \omega)\hat{\tau}_1 + G_3(\mathbf{k}, \omega)\hat{\tau}_3$ with the renormalized quantities determined from the Pauli components of the self energy as $\tilde{\omega} = \omega - \Sigma_0(\mathbf{k}, \tilde{\omega})$, $\tilde{\epsilon}(\mathbf{k}) = \epsilon(\mathbf{k}) + \Sigma_3(\mathbf{k}, \tilde{\omega})$, and $\tilde{\Delta}(\mathbf{k}) = \Delta(\mathbf{k}) + \Sigma_1(\mathbf{k}, \tilde{\omega})$.

It is well know that vertex corrections appreciably alter universal results and the Wiedemann-Franz law for d -wave superconductors^{73,74,75}. In addition, they are crucially important for describing the back-flow needed to restore gauge-invariance in the superconducting state and appreciably alter the fully-symmetric A_{1g} response over a wide range of frequencies⁷⁶. Again we neglect them to exploit simple symmetry considerations. Therefore we only consider σ_{xx}, σ_{zz} and the B_{1g} and B_{2g} Raman response. The reader is referred to Refs.^{73,74,75,76} where these issues have been addressed at length.

The self energy is usually broken into an inelastic term, such as due to phonons or spin-fluctuations, and an elastic term due to scattering from impurities: $\hat{\Sigma} = \hat{\Sigma}^{inelastic} + \hat{\Sigma}^{elastic}$ ⁷⁷. Since the integrand in Eq. (20) is weighted out for small frequencies and since $\Sigma''_{1,3}(\mathbf{k}, \tilde{\omega})$ coming from inelastic scattering are odd functions of frequency while $\Sigma''_0(\mathbf{k}, \tilde{\omega})$ is even, we only retain Σ_0 . If one considers s -wave impurity scattering in the Born or unitary limit, then $\Sigma_{1,3}^{elastic}$ can be neglected as well. However generally in other limits and in particular if the impurity potential is anisotropic as it should be in correlated systems, one must keep these terms as well^{73,74,77}.

In the next subsection the role of disorder in determining the asymptotic low temperature limit of the results functions is considered, and then in the following subsection, inelastic scattering from spin fluctuations is used to determine the full temperature dependence below T_c .

B. Disorder

We first consider scattering from point-like impurities to determine the low temperature limit of the response functions in the superconducting state. For s -wave impurity scattering $\tilde{\omega} = \omega - \Gamma \frac{\bar{g}_0}{c^2 - \bar{g}_0^2}$, with $\bar{g}_0 = \frac{1}{i} \langle \frac{\tilde{\omega}}{\tilde{\omega}^2 - \Delta^2(\mathbf{k})} \rangle$, $\Gamma = \frac{n_i}{\pi N_F}$, n_i the density of impurities, and c the phase shift⁴². The self energy is determined self-consistently for temperatures below $T^* \sim n_i$ due to the formation of a bound-state impurity band at the Fermi level. In this limit, the solution may be expanded for small frequencies as $\tilde{\omega} = a\omega + i\gamma_0 + ib\omega^2$, with a, b and γ_0 determined from

the impurity concentration and magnitude of the phase shift⁴³. Performing the standard integrals in Eq. (20) yields in the limit of low temperatures $T \ll T^*$

$$\begin{aligned} & \left(\frac{\sigma'_{\alpha,\beta}(T \ll T^*)}{\partial \chi''_{\gamma,\gamma}(T \ll T^*)/\partial \Omega} \right) = -N_F \int dx \frac{\partial f(x)}{\partial x} \\ & \times \left\{ \gamma_0^2 I_{3/2,0}^{\chi_{\gamma,\gamma},\sigma_{\alpha,\beta}} + x^2 \left[2b\gamma_0 I_{3/2,0}^{\chi_{\gamma,\gamma},\sigma_{\alpha,\beta}} + I_{5/2,0}^{\chi_{\gamma,\gamma},\sigma_{\alpha,\beta}} \right. \right. \\ & \times \left(\frac{15}{2} a^2 \gamma_0^2 - 3b\gamma_0^3 \right) - \frac{15}{2} a^2 \gamma_0^4 I_{7/2,0}^{\chi_{\gamma,\gamma},\sigma_{\alpha,\beta}} \\ & \left. \left. - \frac{5}{2} a^2 \gamma_0^2 c^{\chi,\sigma} I_{7/2,1}^{\chi_{\gamma,\gamma},\sigma_{\alpha,\beta}} \right] \right\}, \end{aligned} \quad (21)$$

with the functions

$$\begin{aligned} I_{\nu,\mu}^{\chi_{\gamma,\gamma}} &= \left\langle \frac{\gamma^2(\mathbf{k}) \Delta^\mu(\mathbf{k})}{[\gamma^2 + \Delta^2(\mathbf{k})]^\nu} \right\rangle, \\ I_{\nu,\mu}^{\sigma_{\alpha,\beta}} &= \left\langle \frac{v_\alpha(\mathbf{k}) v_\beta(\mathbf{k}) \Delta^\mu(\mathbf{k})}{[\gamma^2 + \Delta^2(\mathbf{k})]^\nu} \right\rangle, \end{aligned} \quad (22)$$

and the constant $c^{\chi,\sigma} = 2, 0$ for the Raman response and conductivity, respectively due to the different coherence factors. Eqs. (21 - 22) reduce to those found in Ref.⁷⁸ for the case of the $a - b$ plane conductivity. The functions $I_{\nu,\mu}^{\chi,\sigma}$ are straightforward to compute for a cylindrical FS and $\Delta(\mathbf{k}) = \Delta_0 \cos(2\phi)$. For resonant impurity scattering ($c = 0$), $a = 1/2$, $b = -\frac{1}{8\gamma_0}$, and γ_0 is determined self-consistently via $\gamma_0 = \sqrt{\frac{\pi \Gamma \Delta_0}{2 \ln(4\Delta_0/\gamma_0)}}$ ⁴³. Eqs. (21-22) then yield:

$$\sigma'_{xx}(T \ll T^*) = \frac{ne^2}{m\pi\Delta_0} \left[1 + \frac{\pi^2 T^2}{12 \gamma_0^2} \right], \quad (23)$$

$$\sigma'_{zz}(T \ll T^*) = \frac{ne^2}{m\pi\Delta_0} 2 \frac{v_z^2 \gamma_0^2}{v_F^2 \Delta_0^2} \left[1 - \frac{\pi^2 T^2}{12 \gamma_0^2} \right], \quad (24)$$

$$\frac{\partial \chi''_{B_{2g}}}{\partial \Omega}(T \ll T^*) = \frac{2N_F}{\pi\Delta_0} b_2^2 \left[1 + \frac{\pi^2 T^2}{36 \gamma_0^2} \right], \quad (25)$$

$$\begin{aligned} \frac{\partial \chi''_{B_{1g}}}{\partial \Omega}(T \ll T^*) &= \frac{2N_F}{\pi\Delta_0} b_1^2 \frac{\gamma_0^2}{\Delta_0^2} \ln(4\Delta_0/\gamma_0) \\ &\times \left[1 - \frac{\pi^2 T^2}{12 \gamma_0^2} \right], \end{aligned} \quad (26)$$

where n is the 2D electron density. Eq. (23) for the in-plane conductivity has been derived several times^{43,73,78,79}, and Eqs. (25-26) for the Raman slope are identical to those found in Ref.⁴⁸. The result for the out-of-plane conductivity for $T = 0$ is also in agreement with the result from Ref.¹¹, but the temperature dependent variation has not been presented before. We note as in Refs.^{33,43,48,73,78,79} that both the in-plane conductivity and the B_{2g} Raman slope are universal numbers for resonant scattering independent of the strength of the scattering, while both the c -axis conductivity and the B_{1g} Raman slope depend on γ_0 . The γ_0 dependence does not appear in the c -axis conductivity if the c -axis hopping

is taken as a constant independent of direction around the FS^{11,80}. The temperature dependencies are *positive* for both the in-plane conductivity and the B_{2g} slope, but are *negative and identical* for the out-of-plane conductivity and the B_{1g} slope, giving a peak at zero T for the latter pair. We note that this result is in agreement with the rise of the c -axis conductivity recently observed in $\text{YBa}_2\text{Cu}_3\text{O}_{6.95}$ at low temperatures⁴⁷.

In the limit of higher temperatures $T_c \gg T \gg T^*$ where the DOS does not have an impurity induced weight at the Fermi level and matches the DOS from the clean limit, the self consistency is not required for the self energy and Eq. (20) can be rewritten as

$$\begin{aligned} & \left(\frac{\sigma'_{\alpha,\beta}(T^* \ll T \ll T_c)}{\partial \chi''_{\gamma,\gamma}(T^* \ll T \ll T_c)/\partial \Omega} \right) = \\ & -2N_F \int dx \frac{\partial f(x)}{\partial x} \text{Im} \left[\frac{1}{\Omega - i/\tau(x)} \right] \\ & \times \left\langle \left(\frac{v_\alpha(\mathbf{k}) v_\beta(\mathbf{k})}{\gamma^2(\mathbf{k})} \right) \text{Re} \left[\frac{x}{\sqrt{x^2 - \Delta(\mathbf{k})^2}} \right] \right\rangle, \end{aligned} \quad (27)$$

with $1/\tau(x) = -2\Sigma_0''(x)$. This is a generalization of the results obtained in Refs.^{13,14,43} to the case of Raman and optical conductivity. We note that for d - wave superconductors in the resonant limit, the impurity scattering rate depends strongly on frequency

$$1/\tau(\omega \rightarrow 0) = \frac{\pi^2 \Gamma \Delta_0}{2\omega} \frac{1}{\ln^2(4\Delta_0/\omega)}, \quad (28)$$

as shown in Ref.⁴³, which yields

$$\begin{aligned} & \left(\frac{\sigma'_{\alpha,\beta}(T^* \ll T \ll T_c)}{\partial \chi''_{\gamma,\gamma}(T^* \ll T \ll T_c)/\partial \Omega} \right) = \\ & -\frac{4N_F}{\pi^2} \frac{T^2}{\Gamma \Delta_0} \int dz z^2 \frac{e^z}{(e^z + 1)^2} \\ & \times \ln^2(4\Delta_0/zT) H^{\sigma_{\alpha,\beta}, \chi_{\gamma,\gamma}}(zT), \end{aligned} \quad (29)$$

with the functions

$$H^{\sigma_{\alpha,\beta}}(x) = \text{Re} \left\langle \frac{v_\alpha(\mathbf{k}) v_\beta(\mathbf{k})}{\sqrt{x^2 - \Delta(\mathbf{k})^2}} \right\rangle, \quad (30)$$

$$H^{\chi_{\gamma,\gamma}}(x) = \text{Re} \left\langle \frac{\gamma^2(\mathbf{k})}{\sqrt{x^2 - \Delta(\mathbf{k})^2}} \right\rangle. \quad (31)$$

Performing the integrals gives for small x gives

$$H^{\chi_{\gamma,\gamma}}(x) = \begin{cases} \frac{x^2}{2\Delta_0^3}, & B_{1g}, \\ \frac{1}{\Delta_0}, & B_{2g}, \end{cases} \quad (32)$$

$$H^{\sigma_{\alpha,\beta}}(x) = \begin{cases} \frac{1}{2\Delta_0}, & \sigma_{xx}, \\ \frac{x^2}{4\Delta_0^3}, & \sigma_{zz}. \end{cases} \quad (33)$$

The remaining integrals in Eq. (29) can be easily performed:

$$\sigma'_{\alpha,\beta}(T^* \ll T \ll T_c) =$$

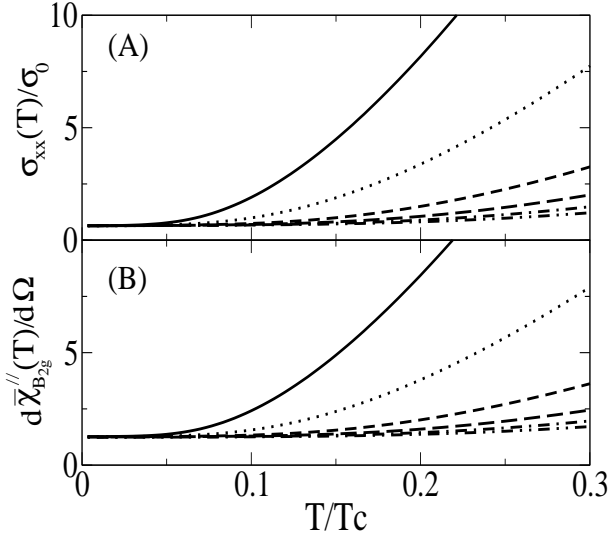


FIG. 4: Temperature dependence of the in-plane conductivity (Panel A) and the B_{2g} Raman slope (Panel B) for resonant scattering and different impurity scattering strengths $\Gamma/\Delta_0 = 0.004, 0.008, 0.016, 0.024$ and 0.04 (solid, dotted, short-dashed, long-dashed, and dotted-dashed lines), respectively, for $\Delta_0/T_c = 4$. Here $\sigma_0 = \pi N_F e^2 v_F^2 / \Delta_0$ and $\chi'' = \chi'' / N_F b_2^2$ are the dimensionless quantities shown.

$$\left\{ \begin{array}{l} \frac{2n\epsilon^2}{3m\Gamma} \left(\frac{T}{\Delta_0}\right)^2 \ln^2\left(\frac{4\Delta_0}{T}\right), \quad \sigma_{xx}, \\ \frac{14\pi^2 n\epsilon^2 v_z^2}{15m\Gamma v_F^2} \left(\frac{T}{\Delta_0}\right)^4 \ln^2\left(\frac{4\Delta_0}{T}\right), \quad \sigma_{zz}, \\ \frac{\partial \chi''_{\gamma,\gamma}(T^* \ll T \ll T_c)}{\partial \Omega} = \end{array} \right. \quad (34)$$

$$\left\{ \begin{array}{l} \frac{4b_2^2 N_F}{3\Gamma} \left(\frac{T}{\Delta_0}\right)^2 \ln^2\left(\frac{4\Delta_0}{T}\right), \quad B_{2g}, \\ \frac{14\pi^2 b_2^2 N_F}{15\Gamma} \left(\frac{T}{\Delta_0}\right)^4 \ln^2\left(\frac{4\Delta_0}{T}\right), \quad B_{1g}. \end{array} \right. \quad (35)$$

The expression for the in-plane conductivity was derived in Ref.⁴³ but to our knowledge the other terms are new. We note the results for σ_{zz} and σ_{xx} in this limit differ from those obtain in Ref.¹⁴, where a frequency independent scattering time was used rather than that of Eq. (28). As a consequence they concluded that $\sigma_{xx,zz}(T) \propto n_{xx,zz}(T)$ with $n_{xx,zz}(T)$ the normal-fluid density which decreases uniformly with temperature in contrast to experiments⁴⁷. From that they concluded that the scattering time must be anisotropic. We note that any frequency dependence of the scattering time would qualitatively change this conclusion.

The results of Eqs. (23-24) and (32-35) imply that the SS relations in the normal state Eq. (16) hold in the superconducting state. The exponent of the low temperature rise *as well as the sign of the correction* do obey the general scaling relation, following simply from the interplay of anisotropies of $\Delta(\mathbf{k})$ and the respective vertices.

Again these relations Eqs. (23-24) and (32-35) would be expected to be violated for the same reasons discussed in the normal state in Section II. However additional con-

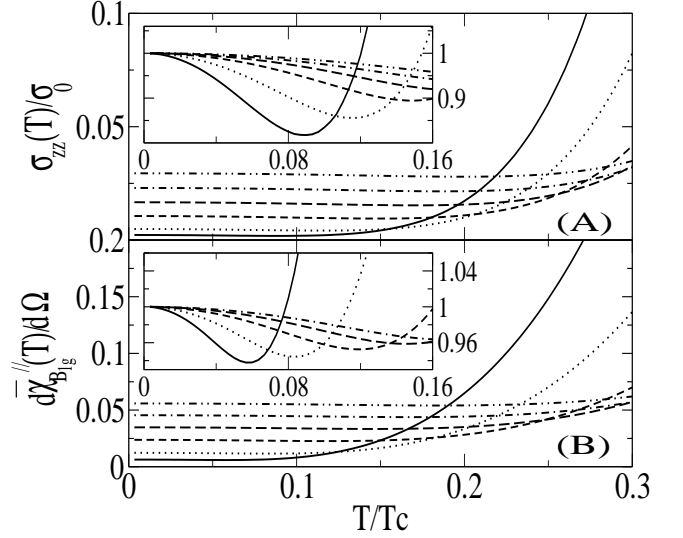


FIG. 5: Temperature dependence of the out-of-plane conductivity (Panel A) and the B_{1g} Raman slope (Panel B) for resonant scattering ($c=0$) and different impurity scattering strengths $\Gamma/\Delta_0 = 0.004, 0.008, 0.016, 0.024$ and 0.04 (solid, dotted, short-dashed, long-dashed, and dotted-dashed lines), respectively, for $\Delta_0/T_c = 4$. Here $\sigma_0 = \pi N_F e^2 v_z^2 / \Delta_0$ and $\chi'' = \chi'' / N_F b_1^2$ are the dimensionless quantities shown. Insets: low temperature rise of both σ_{zz} and $\partial \chi'' / \partial \Omega$ (normalized to their zero temperature values) with decreasing temperature.

siderations should be mentioned here as well. It is well known that at low temperatures $T \ll T^*$ the ab -plane conductivity in Y-123 varies as T^α with an exponent $\alpha \leq 1$ ⁴¹ and not T^2 predicted by Eq. (23), and has been found generally to be non-universal in the zero T limit⁸¹. While vertex corrections can address non universal numbers⁷³ and scattering away from the unitary limit changes α from 1 ^{44,81}, systematic agreement has not been reached at low temperatures. To address this discrepancies, recently Atkinson and Hirschfeld⁸² have shown that a reduced ab -plane conductivity emerges at low temperatures when real-space variations of the order parameter in the neighborhood of the impurities and impurity interference effects are consider in a semiclassical Bogolubov - de Gennes framework. These effects are not captured in the self consistent T -matrix approach and are thus beyond the scope of the present manuscript. It is not immediately clear how the changes in $\sigma_{ab}(T)$ are manifest in other response functions considered in this manuscript and how the derived scaling relations are affected. Our approach should be valid at not too low temperatures where deviations of the conductivity from the unitary limit results are found.

The response for $T \ll T_c$ is calculated by numerically solving Eq. 20 and the corresponding self-consistent equations to determine the self energies. The results for $\sigma_{xx}(T)$, $\partial \chi''_{B_{2g}}(T) / \partial \Omega$, and $\sigma_{zz}(T)$, $\partial \chi''_{B_{1g}}(T) / \partial \Omega$ are shown in Figures 4 and 5, respectively, for resonant scattering and different values of the impurity scattering

strengths Γ/Δ_0 . Generally at higher temperatures $T > T^*$ all quantities increase rapidly with temperature, rising as T^2 and T^4 for σ_{xx} , $\partial\chi_{B_{2g}}/\partial\Omega$ and σ_{zz} , $\partial\chi_{B_{1g}}/\partial\Omega$, respectively. The rise of the c -axis conductivity and the B_{1g} Raman slope at low temperatures shown in the insets of Fig. 5 are generally on the order of a few percent for the parameters shown. This height rises for smaller values of Γ but onsets at smaller temperatures due to the concomitant reduction in T^* . In particular, the rise and the onset of the c -axis conductivity low temperature maximum for $\text{YBa}_2\text{Cu}_3\text{O}_{6.95}$ ⁴⁷ cannot be adequately reproduced. There are as yet no Raman measurements to compare to, and thus it would be extremely useful to have data on a wide range of compounds and doping levels as well as a systematic check of impurity doping effects to test these results.

C. Spin fluctuations

The different rate of descent of the response functions below T_c has an interesting consequence on the conductivity peak seen in ab -plane measurements and the lack of peak seen in c -axis measurements. Ref.⁴³ included inelastic scattering from spin fluctuations in RPA to reproduce the ab -peak in the conductivity observed in Ref.^{40,41}. In Refs.^{14,43} it was shown that Eq. (27) for the conductivities for $T_c \gg T \gg T^*$ may be reexpressed in terms of the normal qp density which can be generalized as

$$\sigma_{\alpha,\beta}(T) = \frac{n_{qp}^{\alpha\beta}(T)\epsilon^2}{m} \bar{\tau}, \quad (36)$$

with

$$n_{qp}^{\alpha,\beta}(T) = \frac{1}{v_F^2} \int d\omega \left\langle \text{Re} \left[\frac{v_\alpha(\mathbf{k})v_\beta(\mathbf{k})\omega}{\sqrt{\omega^2 - \Delta(\mathbf{k})^2}} \right] \right\rangle \left[-\frac{\partial f}{\partial\omega} \right] \quad (37)$$

the projected normal quasiparticle density. The average $\bar{\tau}$ is derived from the frequency-dependent $\tau(\omega)$ and the superconducting DOS $N(\omega)$ as

$$\bar{\tau} = \frac{\int d\omega N(\omega)(-\partial f/\partial\omega)\tau(\omega)}{\int d\omega N(\omega)(-\partial f/\partial\omega)}. \quad (38)$$

Similarly one can re-express the Raman slopes in the same fashion:

$$\partial\chi_{\gamma,\gamma}''(T)/\partial\Omega = n_{qp}^{R,\gamma\gamma}(T)\bar{\tau}, \quad (39)$$

with

$$n_{qp}^{R,\gamma\gamma}(T) = \int d\omega \left\langle \text{Re} \left[\frac{\gamma^2(\mathbf{k})\omega}{\sqrt{\omega^2 - \Delta(\mathbf{k})^2}} \right] \right\rangle \left[-\frac{\partial f}{\partial\omega} \right] \quad (40)$$

the Raman projected normal qp density. For a $d_{x^2-y^2}$ gap, from the results of Eqs. (28-31) the projected qp densities at low T vary as T for n_{qp}^{xx} , $n_{qp}^{R,B_{2g}}$ and T^3 for

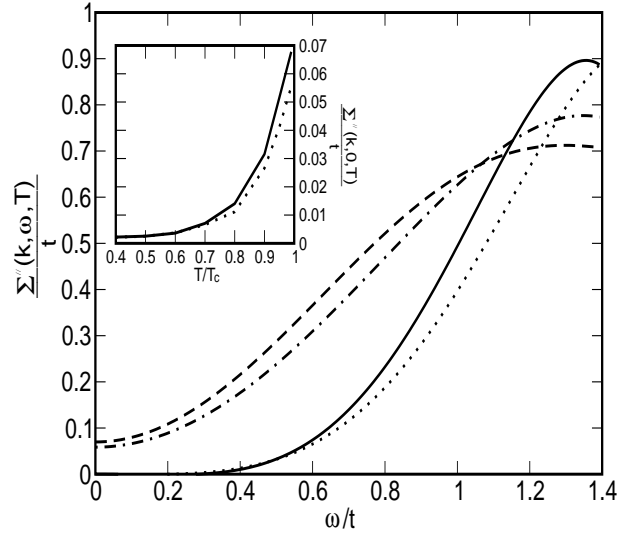


FIG. 6: Frequency dependence of the imaginary part of the $\hat{\tau}_0$ self energy $\Sigma''_0(\mathbf{k}, \omega, T)$ normalized to the hopping overlap t as a function of frequency and temperature for different points in the BZ. The solid line and dotted line are for $T = 0.5T_c$ for gap maximum $\mathbf{k} = (\pi/a, 0)$ and gap node $(\pi/2a, \pi/2a)$ point, respectively, while the dashed and dot-dashed lines correspond to the gap max and gap node points at T_c . The inset shows the zero frequency part of Σ''_0 as a function of temperature.

n_{qp}^{zz} , $n_{qp}^{R,B_{1g}}$, respectively. If the scattering time τ were independent of frequency, then n_{qp} gives the full temperature dependence and thus σ_{xx} , $\partial\chi_{B_{2g}}''/\partial\Omega$ would vary linearly with T and σ_{zz} , $\partial\chi_{B_{1g}}''/\partial\Omega$ would vary as T^3 . Ref.¹⁴ used this result for σ_{zz} and argued that T^3 accurately fit the data for $T > 40K$, but they could not explain the rise at low T . However, the impurity scattering rate as well as the scattering due to inelastic collisions, such as spin fluctuations, depend on momentum and strongly depend on both temperature and frequency. The latter is crucially needed in order to explain the peak in the ab -plane conductivity.

Refs.^{42,43,74} utilized calculations of the inelastic scattering due to spin fluctuations in the 2D Hubbard model in the Random Phase approximation (RPA) for $U = 2t$ to describe the dc and IR conductivity and the frequency dependent Raman response. The lifetime calculated for $U = 2t$ and $\Delta_0/T_c = 3-4$ ⁸³ was found to give reasonable agreement with the transport lifetime determined from conductivity measurements in Y-123⁴¹ and gave reasonable agreement with the ab -plane conductivity peak⁴³, ab -plane IR conductivity response⁴², and simultaneously the ab -plane IR and the B_{1g} and B_{2g} Raman response in Bi-2212⁷⁴. We therefore use this approach to calculate the temperature dependence of the response functions for all temperatures below T_c .

In RPA, the self energy Σ_0 is given from the effective potential V as:

$$V(\mathbf{q}, i\Omega) = \frac{3}{2} \frac{\bar{U}^2 \chi_0(\mathbf{q}, i\Omega)}{1 - \bar{U} \chi_0(\mathbf{q}, i\Omega)}, \quad (41)$$

where \bar{U} is a phenomenological parameter [we choose $\bar{U} = 2t$]. $\chi_0(\mathbf{q}, i\Omega)$ is the non-interacting spin susceptibility,

$$\chi_0(\mathbf{q}, i\Omega) = \sum_{\mathbf{k}} \left\{ \frac{a_{\mathbf{k}, \mathbf{k}+\mathbf{q}}^+}{2N} \frac{f(E_{\mathbf{k}+\mathbf{q}}) - f(E_{\mathbf{k}})}{i\Omega - (E_{\mathbf{k}+\mathbf{q}} - E_{\mathbf{k}})} + \frac{a_{\mathbf{k}, \mathbf{k}+\mathbf{q}}^-}{4N} \left[\frac{1 - f(E_{\mathbf{k}+\mathbf{q}}) - f(E_{\mathbf{k}})}{i\Omega + E_{\mathbf{k}+\mathbf{q}} + E_{\mathbf{k}}} - \frac{1 - f(E_{\mathbf{k}+\mathbf{q}}) - f(E_{\mathbf{k}})}{i\Omega - E_{\mathbf{k}+\mathbf{q}} - E_{\mathbf{k}}} \right] \right\}. \quad (42)$$

Here $E_{\mathbf{k}}^2 = \epsilon_{\mathbf{k}}^2 + \Delta_{\mathbf{k}}^2$ and the coherence factors are $a_{\mathbf{k}, \mathbf{k}+\mathbf{q}}^{\pm} = 1 \pm \frac{\epsilon_{\mathbf{k}+\mathbf{q}}\epsilon_{\mathbf{k}} + \Delta_{\mathbf{k}}\Delta_{\mathbf{k}+\mathbf{q}}}{E_{\mathbf{k}+\mathbf{q}}E_{\mathbf{k}}}$. This yields a self energy

$$\hat{\Sigma}(\mathbf{k}, i\omega) = - \int \frac{dx}{\pi N} \sum_{\mathbf{q}} \frac{V''(\mathbf{q}, x)}{2E_{\mathbf{k}-\mathbf{q}}} \times \left[\frac{E_{\mathbf{k}-\mathbf{q}}\hat{\tau}_0 + \epsilon_{\mathbf{k}-\mathbf{q}}\hat{\tau}_3 + \Delta_{\mathbf{k}-\mathbf{q}}\hat{\tau}_1}{E_{\mathbf{k}-\mathbf{q}} + x - i\omega} [n(x) + f(-E_{\mathbf{k}-\mathbf{q}})] - \frac{-E_{\mathbf{k}-\mathbf{q}}\hat{\tau}_0 + \epsilon_{\mathbf{k}-\mathbf{q}}\hat{\tau}_3 + \Delta_{\mathbf{k}-\mathbf{q}}\hat{\tau}_1}{-E_{\mathbf{k}-\mathbf{q}} + x - i\omega} [n(x) + f(E_{\mathbf{k}-\mathbf{q}})] \right], \quad (43)$$

with n the Bose factor.

The imaginary part of the $\hat{\tau}_0$ self energy $\Sigma_0''(\mathbf{k}, \omega, T)$ normalized to the hopping overlap t as a function of frequency and temperature for different points in the BZ is shown in Fig. (6). Here we have used the band structure $\epsilon_{\mathbf{k}}$ as in (A4) in the appendix with $t'/t = 0.45$ and a filling $n = 0.88$, $U = 2t$, and a $d_{x^2-y^2}$ energy gap $\Delta_{\mathbf{k}} = \Delta_0[\cos(k_x a) - \cos(k_y a)]/2$ with $\Delta_0/t = 0.4 = 4T_c/t$. The solid line and dotted line shows the frequency dependence of Σ'' at a temperature $T = 0.5T_c$ for gap maximum $\mathbf{k} = (\pi/a, 0)$ and gap node $(\pi/2a, \pi/2a)$, respectively, while the dashed and dot-dashed lines correspond to the gap max and gap node points at T_c . The differences for the gap maximum and gap node points are not too strong and can be adequately fit with a threshold behavior $\sim (\omega - 3\Delta(\mathbf{k}))^3$ plus a temperature dependent part which also depends on momentum. The inset shows the zero frequency part of Σ_0'' as a function of temperature. Except for low temperatures where the nodal properties of the interaction govern the behavior, the momentum dependence of the self energy is weak and can be adequately modelled by a temperature dependent $\sim T^3$ term plus a frequency dependent part $\sim \omega^3$.

In an effort to address the temperature dependence of these quantities, we employ a simple parameterized fit to the numerical results for $1/\tau_{\mathbf{k}}(\omega, T) = -2\Sigma_0''(\mathbf{k}, \omega, T)$ determined from Eq. (44) and Fig. (8) and add that to the elastic contribution calculated in the last section. Assuming Matthiessen's law to hold in this case neglects vertex corrections and the joint influence of disorder on the spin fluctuations and vice-versa, but for weak disorder should be sufficient to capture the qualitative behavior of various quantities derived on the FS.

The results for the four response functions derived from Eq. (20) are shown in Figures 7 and 8. Both the in-plane conductivity (Fig. 7A) and the B_{2g} Raman slope (Fig. 7B) possess a peak near $T \sim 0.3T_c$ for $\Gamma/\Delta_0 = 0.004$ which decreases in height and moves to higher temperatures for increasing impurity scattering. It is important to emphasize that this peak is not related to coherence

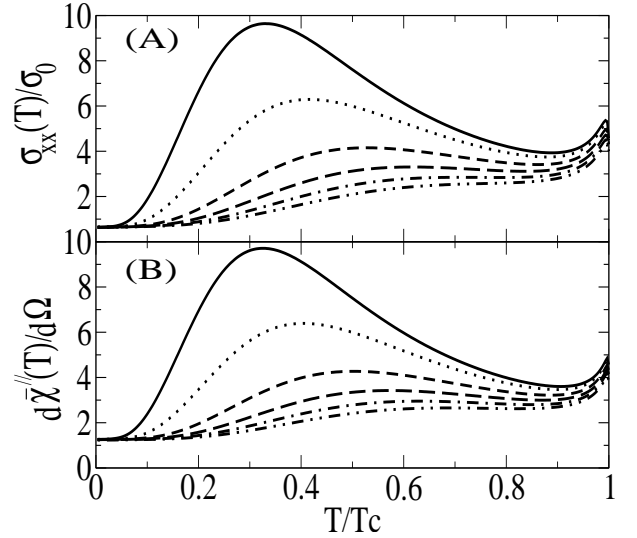


FIG. 7: Temperature dependence of the in-plane conductivity (Panel A) and the B_{2g} Raman slope (Panel B) including inelastic spin fluctuations and resonant impurity scattering for different impurity scattering strengths $\Gamma/\Delta_0 = 0.004, 0.008, 0.016, 0.024$ and 0.04 (solid, dotted, short-dashed, long-dashed, and dotted-dashed lines), respectively, for $\Delta_0/T_c = 4$. Here $\sigma_0 = \pi N_F e^2 v_F^2 / \Delta_0$ and $\bar{\chi}'' = \chi'' / N_F b_2^2$ are the dimensionless quantities shown.

effects and is a simple balance of fall-off of the inelastic scattering rate $\sim T^3$ and the rise of the impurity scattering rate $\sim 1/T$ at low temperatures. The sum of these scattering rates is multiplied by the normal qp density $\propto T$ at low temperatures, as shown in Eqs. (29) and (35), and therefore σ_{xx} and $\partial \bar{\chi}''_{B_{2g}} / \partial \Omega$ vary as $1/T^2$ for $T^* < T < T_c$ and approach a universal constant in the zero temperature limit.

However, no corresponding peak is found for both the out-of-plane conductivity (Fig. 8A) and B_{1g} Raman slope (Fig. 8B), in agreement with experimental obser-

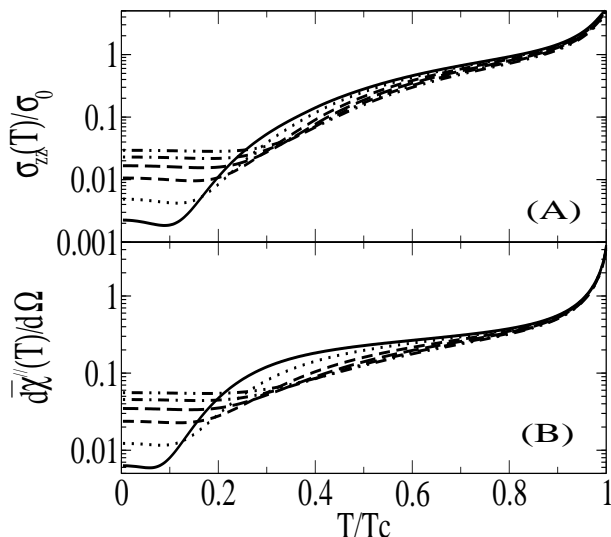


FIG. 8: Temperature dependence of the out-of-plane conductivity σ_{zz} (Panel A) and the B_{1g} Raman slope (Panel B) including inelastic spin fluctuations and resonant impurity scattering for different impurity scattering strengths $\Gamma/\Delta_0 = 0.004, 0.008, 0.016, 0.024$ and 0.04 (solid, dotted, short-dashed, long-dashed, and dotted-dashed lines), respectively, for $\Delta_0/T_c = 4$. Here $\sigma_0 = \pi N_F e^2 v_F^2 / \Delta_0$ and $\bar{\chi}'' = \chi'' / N_F b_1^2$ are the dimensionless quantities shown.

vations. The curves simply show a rapid fall off of both quantities for $T < T_c$ and a small rise of both quantities which onsets at T^* and reaches a zero temperature maximum as shown in Fig. 5. The main difference is due to the behavior of zone-axis projected qp density, which varies as T^3 at low temperatures, with a factor of T coming from the nodes and the additional T^2 coming from the matrix elements. This compensates the $1/T^3$ rise of the qp inelastic lifetime, and both σ_{zz} and $\partial\chi''_{B_{1g}}/\partial\Omega$ vary as T^μ for $T \gg T^*$ with μ dependent on the strength of the impurity scattering, and rise for $T \ll T^*$, as shown in Fig. (5). For example, for the parameters chosen in Fig. (8), the exponent μ for $0.3T_c < T < 0.9T_c$ for the c -axis conductivity $\sigma_{zz}(T)$ varies from 2.7 to 3.4 for increasing impurity scattering. If the frequency dependence of the scattering rate were neglected, then a universal exponent $\mu = 3$ would emerge¹⁴. Therefore it would be highly useful if further systematic checks were performed and Raman data were available to compare to the conductivity and the theoretical predictions.

IV. SUMMARY AND CONCLUSIONS

In summary, based on symmetry arguments we have demonstrated how the relaxational behavior of the qp in the cuprates should manifest itself in the various experiments and how the results are expected to be interrelated. Therefore, a single framework may relate the optically-derived qp scattering rates to transport measurements

to infer charge dynamics on different regions of the Brillouin zone. Using forms for the interlayer hopping and qp self energy consistent with empirical evidence, a variant of the SS relation was shown to relate the zone-diagonal and zone-axis transport properties measured by DC conductivity and the slope of the Raman response in the normal state, in agreement with experimental observations in Bi-2212 and Y-123, but not La-214. Violations of the derived scaling relations were discussed most pointedly in connection with the role of vertex corrections.

The “scattering ratios” show power-law behavior for the Raman response which can be reasonably accounted for in several models near optimal doping. However no single model can adequately describe the data over the entire doping range, indicating that additional physics related to strong correlations is required²⁶. A presence of a pseudogap is discussed in simple symmetry terms, revealing that the B_{1g} Raman scattering and c -axis conductivity are most affected in agreement with experiments. This is a consequence of a loss of qp coherence near the BZ axes.

The data on La-214 over a wide range of doping is inconsistent with the simple models for qp scattering discussed herein. A connection can be made between the in-plane conductivity and Raman response in light of stripe orientation. However more work is clearly needed to address this point.

We note that a quantitative connection between the magnitude and temperature dependence of the qp self energy derived from ARPES, the in-plane and out-of-plane conductivity, and the Raman response can only be undertaken with an understanding of the role of vertex corrections.

In the superconducting state, a similar SS relation is found which arises from the momentum dependence of the energy gap and conductivity and Raman matrix elements. In particular, we found that the a zero temperature peak is predicted to arise in σ_{zz} and $\partial\chi''_{B_{1g}}/\partial\Omega$ without the presence of a maximum near $0.3T_c$ found for σ_{xx} and $\partial\chi''_{B_{1g}}/\partial\Omega$. The results are in rough, qualitative agreement with the available data for σ_{zz} but the strength of the elastic scattering cannot simultaneously account for in-plane and out-of-plane conductivities. However, the simple model presented does not account for anisotropies in impurity scattering, known to arise for point-like scatterers in correlated materials, or impurity interference effects. In particular, it would be useful to determine whether the approach followed by Atkinson and Hirschfeld⁸² would remedy the agreement to the c -axis conductivity rise at low temperatures. Unfortunately, Raman data in the superconducting state to further test the theory is lacking. In particular, it would be extremely useful to determine if the deviations from the derived SS relation observed in the normal state of La-214 carry over into the superconducting state.

The agreement of the derived SS relations in both the superconducting and normal states with the available data on Bi-2212 and Y-123 indicate that the in-plane

momentum is at least partially conserved in c -axis transport over the entire doping range studied. This shows that in principle a comparison of Raman and transport could eventually contribute to the solution of the c -axis transport problem.

Acknowledgments

The author would like to thank R. Hackl, F. Venturini, G. Blumberg, A. Kampf and X.-G. Wen for numerous discussions, and gratefully acknowledges support from NSERC, PREA and from the Alexander von Humboldt Foundation.

APPENDIX A

We start by considering a four band model for the CuO_2 plane with $Cu_{3d} - O_{p_{x,y}}$ hopping amplitude t_{pd} , $Cu_{4s} - O_{p_{x,y}}$ hopping amplitude t_{ps} , $O_{p_x} - O_{p_y}$ hopping amplitude t_{pp} , and c -axis $Cu_{4s} - Cu_{4s}$ amplitude t_s , respectively:

$$\begin{aligned}
H &= \epsilon_d \sum_{\mathbf{n},\sigma} d_{\mathbf{n},\sigma}^\dagger d_{\mathbf{n},\sigma} + \epsilon_s \sum_{\mathbf{n},\sigma} s_{\mathbf{n},\sigma}^\dagger s_{\mathbf{n},\sigma} \\
&- t_{pd} \sum_{\mathbf{n},\delta,\sigma} P_\delta (d_{\mathbf{n},\sigma}^\dagger a_{\mathbf{n},\delta,\sigma} + h.c.) \\
&- t_{pp} \sum_{\mathbf{n},\delta,\delta',\sigma} P'_{\delta,\delta'} a_{\mathbf{n},\delta,\sigma}^\dagger a_{\mathbf{n},\delta',\sigma} \\
&- t_{ps} \sum_{\mathbf{n},\delta,\sigma} P''_\delta (s_{\mathbf{n},\sigma}^\dagger a_{\mathbf{n},\delta,\sigma} + h.c.) \\
&- t_s \sum_{(\mathbf{n},\mathbf{m}),\sigma} s_{\mathbf{n},\sigma}^\dagger s_{\mathbf{m},\sigma}, \tag{A1}
\end{aligned}$$

where $\epsilon_{s,d} = E_{s,d} - E_p$ represents the charge transfer energy from the oxygen p - to $Cu_{4s,3d}$ orbitals, respectively. Here $s_{\mathbf{n},\sigma}^\dagger, d_{\mathbf{n},\sigma}^\dagger$ creates an $4s, 3d_{x^2-y^2}$ electron, respectively, with spin σ at a copper lattice site \mathbf{n} , while $a_{\mathbf{n},\delta,\sigma}$ annihilates an electron at one of the neighboring oxygen sites $\mathbf{n} + \delta/2$ determined by the unit vector δ assuming the four values, $(\pm 1, 0)$ and $(0, \pm 1)$. The overlap factors P have the following properties: $P_{(1,0)} = P''_{(1,0)} = 1, P_{(0,1)} = P''_{(0,1)} = -1, P'_{\mathbf{x},\mathbf{y}} = P'_{-\mathbf{x},-\mathbf{y}} =$

$1, P'_{-\mathbf{x},\mathbf{y}} = P'_{\mathbf{x},-\mathbf{y}} = -1$, respectively. Lastly the bracket $\langle \dots \rangle$ notes a sum over the nearest neighbor Cu_{4s} sites in the c -direction. Thus c -axis hopping is mediated by the Cu_{4s} orbitals hybridizing with the bonding and anti-bonding pd bands consistent with LDA²².

After Fourier transforming, the Hamiltonian is $H = \sum_{\mathbf{k},\sigma} H_{\mathbf{k},\sigma}$ with

$$\begin{aligned}
H_{\mathbf{k},\sigma} &= \epsilon_d d_{\mathbf{k},\sigma}^\dagger d_{\mathbf{k},\sigma} + \epsilon_s(\mathbf{k}) s_{\mathbf{k},\sigma}^\dagger s_{\mathbf{k},\sigma} \\
&- \{2it_{pd} d_{\mathbf{k},\sigma}^\dagger [a_{x,\mathbf{k},\sigma} s_x(\mathbf{k}) - a_{y,\mathbf{k},\sigma} s_y(\mathbf{k})] + h.c.\} \\
&- \{2it_{ps} s_{\mathbf{k},\sigma}^\dagger [a_{x,\mathbf{k},\sigma} s_x(\mathbf{k}) + a_{y,\mathbf{k},\sigma} s_y(\mathbf{k})] + h.c.\} \\
&- 4t_{pp} s_x(\mathbf{k}) s_y(\mathbf{k}) [a_{x,\mathbf{k},\sigma}^\dagger a_{y,\mathbf{k},\sigma} + h.c.], \tag{A2}
\end{aligned}$$

with $s_\alpha(\mathbf{k}) = \sin(ak_\alpha/2)$ and $\epsilon_s(\mathbf{k}) = \epsilon_s - 2t_{ss} \cos(k_z c)$. Eq. A2 can be diagonalized by defining ‘‘canonical fermions’’⁸⁵:

$$\begin{aligned}
\alpha_{\mathbf{k},\sigma} &= i \frac{s_x(\mathbf{k}) a_{x,\mathbf{k},\sigma} - s_y(\mathbf{k}) a_{y,\mathbf{k},\sigma}}{\mu(\mathbf{k})} \\
\beta_{\mathbf{k},\sigma} &= -i \frac{s_y(\mathbf{k}) a_{x,\mathbf{k},\sigma} + s_x(\mathbf{k}) a_{y,\mathbf{k},\sigma}}{\mu(\mathbf{k})}, \tag{A3}
\end{aligned}$$

where $\mu(\mathbf{k})^2 = s_x^2(\mathbf{k}) + s_y^2(\mathbf{k})$. This gives anti-bonding, bonding bands hybridized with the Cu orbitals. This four-band model can be reduced to an effective one-band model by eliminating the β band and the two bands with high energies $\sim \epsilon_{s,d}$. This is achieved by defining two other sets of canonical fermions and expanding in powers of $t_{pd,pd,ss}/\epsilon_{s,d}$ ⁸⁶. The single-band dispersion is approximately given by

$$\begin{aligned}
\epsilon(\mathbf{k}) &= -2t[\cos(k_x a) + \cos(k_y a)] + 4t' \cos(k_x a) \cos(k_y a) \\
&- 2t'' \cos(2k_x a) \cos(2k_y a) \\
&- t_\perp \cos(k_z c) [\cos(k_x a) - \cos(k_y a)]^2 - \mu, \tag{A4}
\end{aligned}$$

with the identification to lowest order of $t = t_{pp} - t_{pd}^2/\epsilon_d, t' = -t_{pp}/2 + t_{ps}^2/8\epsilon_s, t'' = t_{ps}^2/16\epsilon_s$, and $t_\perp = t_{ss} t_{ps}^2/\epsilon_s^2$. This form for the interplane hopping can also be derived in the framework of the Hubbard model by projecting out the high-lying Cu $4s$ orbitals and the high-lying $d-p$ spin triplets by solving the correlation problem within the unit cell and treating the intercell hopping as a degeneracy lifting perturbation^{13,85}.

¹ A. Damascelli, Z. Hussain, and Z.-X. Shen Rev. Mod. Phys. **75**, 473-541 (2003).
² S. L. Cooper and K. E. Gray, in *Physical Properties of High-Temperature Superconductors IV*, edited by D. M. Ginsberg (World Scientific, Singapore, 1994).
³ S. V. Dordevic, E. J. Singley, D. N. Basov, S. Komiyama, Y. Ando, E. Bucher, C. C. Homes and M. Strongin, Phys. Rev. B **65**, 134511 (2002); S. Tajima, J. Schützmann, S.

Miyamoto, I. Terasaki, Y. Sato, and R. Hauff, Phys. Rev. B **55**, 6051 (1997).
⁴ T. Watanabe, T. Fujii, and A. Matsuda, Phys. Rev. Lett. **79**, 2113 (1997).
⁵ C. Kendziora, M. C. Martin, J. Haartge, L. Mihaly, and L. Forró, Phys. Rev. B **48**, 3531 (1993).
⁶ L. Forró, Phys. Lett. A **179**, 140 (1993).
⁷ D. N. Basov, S. I. Woods, A. S. Katz, E. J. Singley, R. C.

- Dynes, M. Xu, D. G. Hinks, C. C. Homes, and M. Strongin, *Science* **283**, 49 (1999); D. N. Basov, C. C. Homes, E. J. Singley, M. Strongin, T. Timusk, G. Blumberg, and D. van der Marel, *Phys. Rev. B* **63**, 134514 (2001); H. J. A. Molegraaf, C. Presura, D. van der Marel, P. H. Kes, and M. Li, *Science* **295**, 2239 (2002).
- ⁸ J. L. Tallon and J. W. Loram, *Physica C* **349**, 53 (2001).
- ⁹ P. W. Anderson, *The Theory of Superconductivity in the High T_c Cuprates* (Princeton University Press, Princeton, 1997); A. J. Leggett, *Phys. Rev. Lett.* **83**, 392 (1999); M. Turlakov and A. J. Leggett, *Phys. Rev. B* **63**, 64518 (2001).
- ¹⁰ L. B. Ioffe and A. J. Millis, *Science* **285**, 1241 (1999); *Phys. Rev. B* **61**, 9077 (2000); N. Shah and A. J. Millis, *Phys. Rev. B* **64**, 174506 (2001); **65**, 024506 (2001).
- ¹¹ W. Kim and J. P. Carbotte, *Phys. Rev. B* **63**, 054526 (2001); E. Schachinger and J. P. Carbotte, *Phys. Rev. B* **64**, 94501 (2001).
- ¹² P. S. Cornaglia, K. Hallberg, and C. A. Balseiro, *Phys. Rev. B* **63**, 060504 (2001).
- ¹³ T. Xiang and J. M. Wheatley, *Phys. Rev. Lett.* **77**, 4632 (1996).
- ¹⁴ T. Xiang and W. Hardy, *Phys. Rev. B* **63**, 024506 (2000).
- ¹⁵ D. van der Marel, *Phys. Rev. B* **60**, 765 (1999).
- ¹⁶ L. B. Ioffe and A. J. Millis, *Phys. Rev. B* **58**, 11631 (1998).
- ¹⁷ R. Hlubina and T. M. Rice, *Phys. Rev. B* **51**, 9253 (1995); D. Pines and B. Stojković **55**, 8576 (1997); **56**, 11931 (1997); R. Hlubina, *Phys. Rev. B* **58**, 8240 (1998).
- ¹⁸ P. Coleman, A. J. Schofield, and A. M. Tselvik, *Phys. Rev. Lett.* **76**, 1324 (1996); A. T. Zheleznyak, V. M. Yakovenko, H. D. Drew, and I. I. Mazin, *Phys. Rev. B* **57**, 3089 (1998); **59**, 207 (1999); K. G. Sandeman and A. J. Schofield, *Phys. Rev. B* **63**, 094510 (2001).
- ¹⁹ E. Abrahams and C. M. Varma, *Phys. Rev. Lett.* **86**, 4652 (2001); **88**, 139903 (2002).
- ²⁰ A. A. Abrikosov, *Physica C* **258**, 53 (1996).
- ²¹ W. A. Atkinson and J. P. Carbotte, *Phys. Rev. B* **55**, 12748 (1997).
- ²² O. K. Andersen, O. Jepsen, A. I. Liechtenstein, and I. I. Mazin, *Phys. Rev. B* **49**, 4145 (1994); *J. Phys. Chem. Solids* **56**, 1573 (1995).
- ²³ R. Hackl, M. Opel, P. F. Müller, G. Krug, B. Stadlober, R. Nemetschek, H. Berger and L. Forró, *J. Low Temp. Phys.* **105**, 733 (1996).
- ²⁴ G. Blumberg and M.V. Klein, *Journ. of Low Temp. Phys.* **117**, 1001 (1999).
- ²⁵ M. Opel, R. Nemetschek, C. Hoffmann, R. Philipp, P. F. Müller, R. Hackl, I. Tüttö, A. Erb, B. Revaz, E. Walker, H. Berger and L. Forró, *Phys. Rev. B* **61**, 9752 (2000).
- ²⁶ F. Venturini, M. Opel, T. P. Devereaux, J. K. Freericks, I. Tüttö, B. Revaz, E. Walker, H. Berger, L. Forró, and R. Hackl, *Phys. Rev. Lett.* **89**, 107003 (2002).
- ²⁷ C. C. Homes, T. Timusk, D. A. Bonn, R. Liang, W. N. Hardy, *Physica C* **254**, 265 (1995); D. N. Basov, T. Timusk, B. Dabrowski, and J. D. Jorgensen, *Phys. Rev. B* **50**, 3511 (1994).
- ²⁸ see e.g., T. Timusk and B. Statt, *Rep. Prog. Phys.* **62**, 61 (1999).
- ²⁹ A. V. Puchkov, D. N. Basov, and T. Timusk, *J. Phys.: Condens. Matter* **8**, 10049 (1996); N. L. Wang, P. Zheng, T. Feng, G. D. Gu, C. C. Homes, J. M. Tranquada, B. D. Gaulin, and T. Timusk, *Phys. Rev. B* **67**, 134526 (2003).
- ³⁰ J. W. Quilty, S. Tajima, S. Adachi, and A. Yamanaka *Phys. Rev. B* **63**, 100508 (2001).
- ³¹ R. Nemetschek, M. Opel, C. Hoffmann, P. F. Müller, R. Hackl, H. Berger, L. Forró, A. Erb, and E. Walker, *Phys. Rev. Lett.* **78**, 4837 (1997).
- ³² T. P. Devereaux, D. Einzel, B. Stadlober, R. Hackl, D. H. Leach, and J. J. Neumeier *Phys. Rev. Lett.* **72**, 396-399 (1994).
- ³³ T. P. Devereaux and A. P. Kampf, *Int. Journ. Mod. Phys. B* **11**, 2093 (1997).
- ³⁴ C. Kendziora and A. Rosenberg, *Phys. Rev. B* **52**, 9867-9870 (1995); M. Kang, G. Blumberg, M. V. Klein, and N. N. Kolesnikov, *Phys. Rev. Lett.* **77**, 4434 (1996); X. K. Chen, J. G. Naeni, K. C. Hewitt, J. C. Irwin, R. Liang, and W. N. Hardy *Phys. Rev. B* **56**, 513 (1997); A. Sacuto, J. Cayssol, P. Monod, and D. Colson *Phys. Rev. B* **61**, 7122 (2000); M. F. Limonov, S. Tajima, and A. Yamanaka *Phys. Rev. B* **62**, 11859 (2000); S. Sugai and T. Hosokawa, *Phys. Rev. Lett.* **85**, 1112 (2000); K. C. Hewitt and J. C. Irwin, *Phys. Rev. B* **66**, 054516 (2002).
- ³⁵ J.-Y. Genoud, H. J. Trodahl, and A. E. Pantoja, *Sol. State Commun.* **113**, 285 (1999).
- ³⁶ G. Blumberg, M. Kang, M. V. Klein, K. Kadowaki, and C. Kendziora, *Science* **278**, 1427 (1997).
- ³⁷ K. C. Hewitt, N. L. Wang, J. C. Irwin, D. M. Pooke, A. E. Pantoja and H. J. Trodahl, *Phys. Rev. B* **60**, 9943 (1999).
- ³⁸ A weak peak located near 600 cm^{-1} in Bi-2212 appearing above T_c has been a focus of attention and mild controversy. Blumberg *et al.* interpreted the feature as a superconductivity related peak lending credence to a preformed pair scenario of the pseudo-gap³⁶. On the other hand, Hewitt *et al.* investigated isotopically doped systems and found that the peak was absent in oxygenated systems underdoped by Y substitutions³⁷, suggesting that this peak is of phononic origin and related to oxygen disorder in the deoxygenated BiO layers.
- ³⁹ P. Nyhus, S. L. Cooper, and Z. Fisk *Phys. Rev. B* **51**, 15626 (1995); P. Nyhus, S. L. Cooper, Z. Fisk, and J. Sarrao *Phys. Rev. B* **52**, 14308 (1995); *ibid.* **55**, 12488 (1997).
- ⁴⁰ A. Hosseini, R. Harris, S. Kamal, P. Dosanjh, J. Preston, R. Liang, W. N. Hardy, and D. A. Bonn, *Phys. Rev. B* **60**, 1349 (1999).
- ⁴¹ D. A. Bonn, R. Liang, T. M. Riseman, D. J. Baar, D. C. Morgan, K. Zhang, P. Dosanjh, T. L. Duty, A. MacFarlane, G. D. Morris, J. H. Brewer, W. N. Hardy, C. Kallin and A. J. Berlinsky, *Phys. Rev. B* **47**, 11314 (1993).
- ⁴² P. J. Hirschfeld, S. M. Quinlan, and D. J. Scalapino, *Phys. Rev. B* **55**, 12742 (1997).
- ⁴³ P. J. Hirschfeld, W. O. Puttika, and D. J. Scalapino, *Phys. Rev. Lett.* **71**, 3705 (1993); *Phys. Rev. B* **50**, 10254 (1994).
- ⁴⁴ S. Hensen, G. Müller, C. T. Rieck and K. Scharnberg, *Phys. Rev. B* **56**, 6237 (1997).
- ⁴⁵ M. B. Walker and M. F. Smith, *Phys. Rev. B* **61**, 11285 (2000); D. Duffy, P. J. Hirschfeld, and D. J. Scalapino, **64**, 224522 (2001).
- ⁴⁶ M. Matsukawa, T. Mizukoshi, K. Noto, and Y. Shiohara, *Phys. Rev. B* **53**, 6034 (1996).
- ⁴⁷ A. Hosseini, S. Kamal, D. A. Bonn, R. Liang, and W. N. Hardy, *Phys. Rev. Lett.* **81**, 1298 (1998).
- ⁴⁸ W. C. Wu and J. P. Carbotte, *Phys. Rev. B* **57**, 5614 (1998).
- ⁴⁹ B. S. Shastry and B. I. Shraiman, *Phys. Rev. Lett.* **65**, 1068 (1990); *Int. Journ. Mod. Phys. B* **5**, 365 (1991); A. Virosztek and J. Ruvalds, *Phys. Rev. B* **45**, 347 (1992).
- ⁵⁰ J. K. Freericks and T. P. Devereaux, *Phys. Rev. B* **64**, 125110 (2001).
- ⁵¹ J. K. Freericks, T. P. Devereaux, and R. Bulla, *Phys. Rev.*

- B **64**, 233114 (2001).
- ⁵² T. Dahm, D. Manske, and L. Tewordt, Phys. Rev. B **59**, 14740 (1999).
- ⁵³ T. P. Devereaux and A. P. Kampf, Phys. Rev. B **59**, 6411 (1999).
- ⁵⁴ More generally, in off-resonance conditions the vertices can be classified by symmetry in terms of BZ or FS harmonics.
- ⁵⁵ See, e.g., A. Georges, G. Kotliar, W. Krauth, and M. J. Rozenberg Rev. Mod. Phys. **68**, 13-125 (1996).
- ⁵⁶ S. V. Borisenko, A. A. Kordyuk, S. Legner, C. Dürr, M. Knupfer, M. S. Golden, J. Fink, K. Nenkov, D. Eckert, G. Yang, S. Abell, H. Berger, L. Forró, B. Liang, A. Maljuk, C. T. Lin, and B. Keimer, Phys. Rev. B **64**, 094513 (2001); P. V. Bogdanov, A. Lanzara, X. J. Zhou, S. A. Kellar, D. L. Feng, E. D. Lu, H. Eisaki, J.-I. Shimoyama, K. Kishio, Z. Hussain, and Z. X. Shen; *ibid.*, 180505 (2001); A. A. Kordyuk, S. V. Borisenko, T. K. Kim, K. A. Nenkov, M. Knupfer, J. Fink, M. S. Golden, H. Berger, and R. Follath Phys. Rev. Lett. **89**, 077003 (2002).
- ⁵⁷ A. J. Millis, H. Monien, and D. Pines, Phys. Rev. B **42**, 167 (1990); S. Sachdev and J. Ye, Phys. Rev. Lett. **69**, 2411 (1992); R. Haslinger, A. V. Chubukov, and A. Abanov, Phys. Rev. B **63**, 20503 (2001).
- ⁵⁸ C. Castellani, C. Di Castro, and M. Grilli, Phys. Rev. Lett. **75**, 4650 (1995); S. Caprara, M. Sulpizi, A. Bianconi, C. Di Castro, and M. Grilli, Phys. Rev. B **59**, 14980 (1999).
- ⁵⁹ W. Metzner, D. Rohe, S. Andergassen, cond-mat/0303154.
- ⁶⁰ D. Poilblanc, D. J. Scalapino, and W. Hanke, Phys. Rev. Lett. **72**, 884 (1994); A. P. Kampf and T. P. Devereaux, Phys. Rev. B **56**, 2360 (1997).
- ⁶¹ A. Iyengar, J. Stajic, Y.-J. Kao, and K. Levin, Phys. Rev. Lett. **90**, 187003 (2003).
- ⁶² S. A. Kivelson, E. Fradkin, and V. J. Emery, Nature **39** 550 (1998); E. W. Carlson, V. J. Emery, S. A. Kivelson, and D. Orgad, cond-mat/0206217.
- ⁶³ X. G. Wen, Int. J. Mod. Phys. B **4**, 239 (1990); P. A. Lee and N. Nagaosa, Phys. Rev. B **46**, 5621 (1992); X.-G. Wen and P. A. Lee, Phys. Rev. Lett. **80**, 2193 (1998); T. Senthil and M. P. A. Fisher, Phys. Rev. Lett. **86**, 292 (2000); *ibid.* Phys. Rev. B **62**, 7850 (2000).
- ⁶⁴ N. Furukawa, T. M. Rice, and M. Salmhofer, Phys. Rev. Lett. **81**, 3195 (1998); D. Zanchi and H.J. Schulz, Phys. Rev. B **54**, 9509 (1996); *ibid.* **61**, 13609 (2000). C. J. Halboth and W. Metzner, Phys. Rev. B **61**, 7364 (2000); C. Honerkamp, M. Salmhofer, N. Furukawa, and T.M. Rice, Phys. Rev. B **63**, 035109 (2001); A. Katanin and A. P. Kampf, cond-mat/0304189.
- ⁶⁵ C. J. Halboth and W. Metzner, Phys. Rev. Lett. **85**, 5162 (2000); B. Valenzuela and M. A. H. Vozmediano, Phys. Rev. B **63**, 153103 (2001); C. Honerkamp, M. Salmhofer, and T. M. Rice, Eur. Phys. J. B **27**, 127 (2002); A. Neumayr and W. Metzner, Phys. Rev. B **67**, 35112 (2003).
- ⁶⁶ T. Valla, A. V. Feodorov, P. D. Johnson, Q. Li, G. D. Gu, and N. Koshizuka, Phys. Rev. Lett. **85**, 828 (2000).
- ⁶⁷ A. J. Millis and D. Drew, cond-mat/0303018.
- ⁶⁸ F. Venturini, Q.-M. Zhang, R. Hackl, A. Lucarelli, S. Lupi, M. Ortolani, P. Calvani, N. Kikugawa, and T. Fujita, Phys. Rev. B **66**, 060502 (2002); private communication.
- ⁶⁹ A. Ino, C. Kim, M. Nakamura, T. Yoshida, T. Mizokawa, Z.-X. Shen, A. Fujimori, T. Kakeshita, H. Eisaki, and S. Uchida, Phys. Rev. B **62**, 4137 (2000).
- ⁷⁰ A. Lucarelli, S. Lupi, M. Ortolani, P. Calvani, P. Maselli, M. Caprizzi, P. Giura, H. Eisaki, N. Kikugawa, T. Fujita, M. Fujita, and K. Yamada, Phys. Rev. Lett. **90**, 37002 (2003).
- ⁷¹ S. Lupi *et al.*, Phys. Rev. B **62**, 12418 (2000).
- ⁷² D. Munzar and M. Cardona, Phys. Rev. Lett. **90**, 077001 (2003).
- ⁷³ A. C. Durst and P. A. Lee, Phys. Rev. B **62**, 1270 (2000).
- ⁷⁴ T. P. Devereaux and A. P. Kampf, Phys. Rev. B **61**, 1490 (2000).
- ⁷⁵ M. Chiao, R. W. Hill, C. Lupien, L. Taillefer, P. Lambert, R. Gagnon, and P. Fournier, Phys. Rev. B **62**, 3554 (2000).
- ⁷⁶ T. P. Devereaux and D. Einzel, **51**, 16336 (1995); T. P. Devereaux, A. Virosztek and A. Zawadowski, Phys. Rev. B **54**, 12523 (1996).
- ⁷⁷ This treatment does not consider the interplay of disorder and interactions (and particular misses out on the physics of the Anderson-Mott transition) and can only be considered this way in the limit of weak scattering. Efforts to include both disorder and interactions equally in a T-matrix approach have been put forward, most recently in Ref.⁷⁴.
- ⁷⁸ M. J. Graf, S.-K. Yip, J. A. Sauls, and D. Rainer, Phys. Rev. B **53**, 15147 (1996).
- ⁷⁹ M. J. Graf, M. Palumbo, D. Rainer, and J. A. Sauls, Phys. Rev. B **52**, 10588 (1995).
- ⁸⁰ Y. I. Latyshev, T. Yamashita, L. N. Bulaevskii, M. J. Graf, A. V. Balatsky, and M. P. Maley, Phys. Rev. Lett. **82**, 5345 (1999).
- ⁸¹ A. J. Berlinsky, D. A. Bonn, R. Harris and C. Kallin, Phys. Rev. B **61**, 9088 (2000).
- ⁸² W. A. Atkinson and P. J. Hirschfeld, Phys. Rev. Lett. **88**, 187003 (2002).
- ⁸³ S. Quinlan, D. J. Scalapino, and N. Bulut, Phys. Rev. B **49**, 1470 (1994).
- ⁸⁴ S. M. Quinlan, P. J. Hirschfeld, and D. J. Scalapino, Phys. Rev. B **53**, 8575 (1996).
- ⁸⁵ B. S. Shastry, Phys. Rev. Lett. **63**, 1288 (1989); D. C. Mattis, Phys. Rev. Lett. **74**, 3676 (1995).
- ⁸⁶ J. H. Jefferson, H. Eskes, and L. F. Feiner, Phys. Rev. B **45**, 7959 (1992).

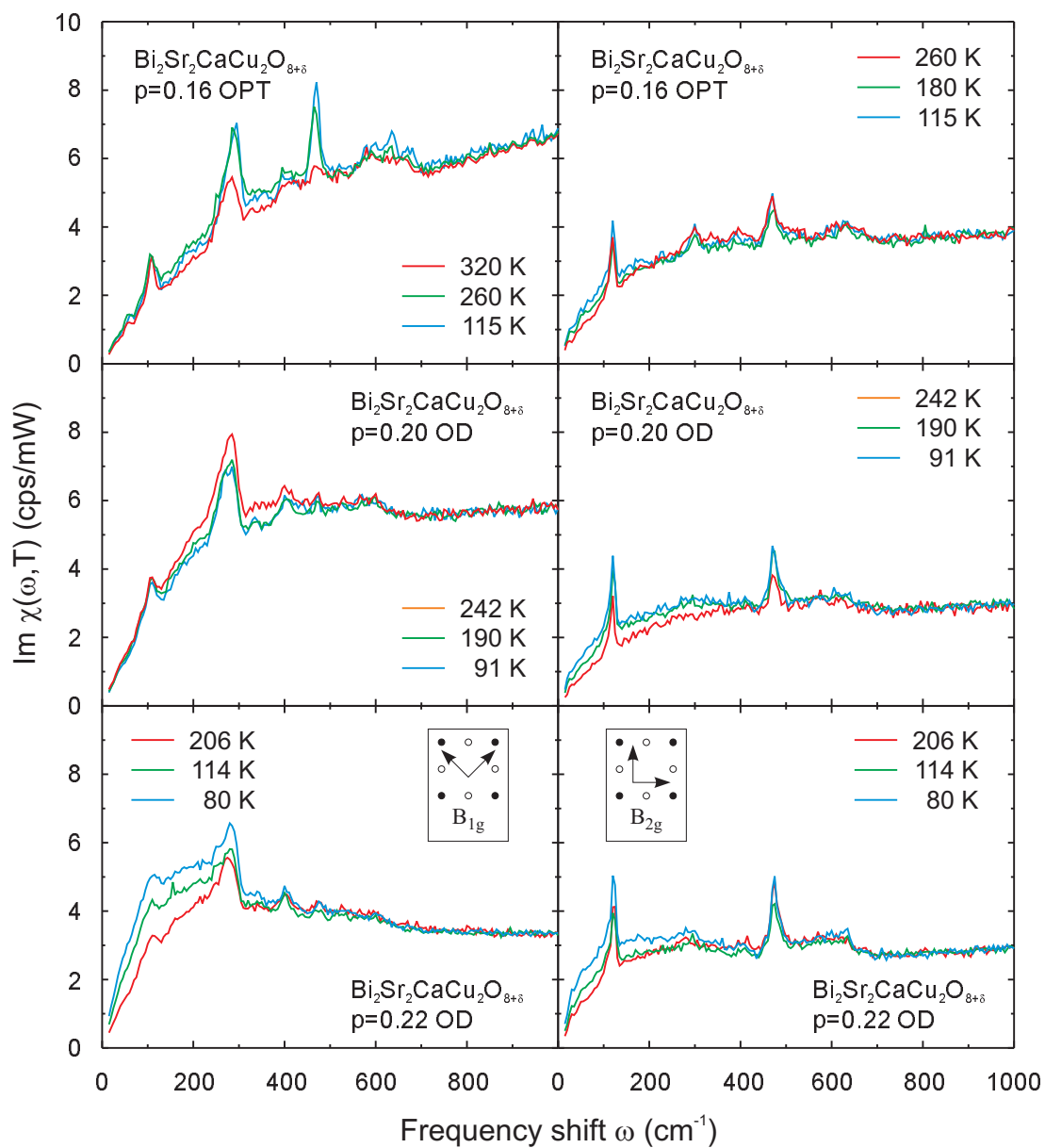


fig1_imchi.cdr